TUDelft

Delft University of Technology

Jamming in soft disk packings

Koeze, D.J.

DOI
10.4233/uuid:02da241b-3580-4342-b610-cf5c26368ab1

Publication date
2022

Document Version
Final published version

Citation (APA)
Koeze, D. J. (2022). *Jamming in soft disk packings*. [Dissertation (TU Delft), Delft University of Technology]. https://doi.org/10.4233/uuid:02da241b-3580-4342-b610-cf5c26368ab1

Important note
To cite this publication, please use the final published version (if applicable).
Please check the document version above.

JAMMING IN SOFT DISK PACKINGS

JAMMING IN SOFT DISK PACKINGS

Proefschrift

ter verkrijging van de graad van doctor
aan de Technische Universiteit Delft,
op gezag van de Rector Magnificus prof. dr. ir. T.H.J.J. van der Hagen,
voorzitter van het College voor Promoties,
in het openbaar te verdedigen op vrijdag 10 juni 2022 om 12.30 uur

door

Dionysius Johannes KOEZE

Natuur- en Wiskundig ingenieur,
Technische Universiteit Delft,
geboren te Woerden, Nederland.

Dit proefschrift is goedgekeurd door de

promotor: dr. B.P. Tighe
promotor: prof. dr. ir. T.J.H. Vlugt

Samenstelling promotiecommissie:

Rector Magnificus,	voorzitter
prof. dr. ir. T.J.H. Vlugt	Technische Universiteit Delft, promotor
dr. B.P. Tighe	Technische Universiteit Delft, promotor

Onafhankelijke leden:

prof. dr. ir. J.T. Padding	Technische Universiteit Delft
dr. P.E. Boukany	Technische Universiteit Delft
prof. dr. J.H. Snoeijer	Universiteit Twente
prof. dr. S. Luding	Universiteit Twente
prof. dr. D.J.E.M. Roekaerts	Technische Universiteit Delft

Keywords:	rigidity percolation, phase transitions, complex fluids, elasticity
Printed by:	Ridderprint - www.ridderprint.nl
Front & Back:	Design based on the work "City Dust KD" by Jeroen Kramer (jeroen.kramer@rietveldacademie.nl). *One can see order through disorder.*

An electronic version of this dissertation is available at
http://repository.tudelft.nl/.

CONTENTS

SUMMARY

This thesis considers the mechanical properties of amorphous solids such as foams, emulsions, and granular media. Each of these systems consists of "particles" (bubbles, droplets, grains) in a dense, disordered structure. As a system is compressed, it eventually forms enough contacts between particles that it can support a load, including shearing stresses. We say that it has *jammed*. A major theoretical challenge is to describe material properties in the vicinity of this non-equilibrium phase transition.

Jamming has been widely studied in the context of a specific model, namely non-Brownian packings of soft frictionless disks or spheres. The particles repel when they overlap, and otherwise do not interact. They come in two distinct sizes to prevent crystallization; by convention the concentration and diameter ratio of the species are fixed to specific values. Little is known about the nature of the jammed solids that result when these restrictions are lifted. This is a significant knowledge gap, because bubbles, droplets, and grains routinely experience some degree of attraction to their neighbors (e.g. due to depletion interactions or capillary bridges), and their size distribution can vary considerably. Hence the goal of this thesis is to determine how the soft sphere model jams (i) when the degree of attraction between particles is varied, and (ii) when the size and number ratio of particles in a repulsive bidisperse packing is varied.

Attraction.— First, we study how soft particles with an attractive shell become rigid. By analyzing the percolation of rigid clusters of particles, we present evidence for two distinct jamming scenarios. Strongly attractive systems undergo a continuous transition in which rigid clusters grow and ultimately diverge in size at a critical packing fraction. Purely repulsive and weakly attractive systems jam via a first order transition, with no growing cluster size. We further show that the weakly attractive scenario is a finite size effect, so that for any nonzero attraction strength, a sufficiently large system will fall in the strongly attractive universality class. We therefore expect attractive jamming to be generic in the laboratory and in nature. Second, we probe the elasticity of the strongly attractive solid. By treating the jamming point as a critical point, we exploit critical scaling analysis to determine the shear modulus, bulk modulus, and coordination of marginal solids close to the sticky jamming point. We find that each observable differs not just quantitatively but also qualitatively from the purely repulsive case.

Size and number ratio.—We systematically map out the jamming transition of 2D bidisperse mixtures of disks in the hard particle limit. The critical volume fraction and multiple structural and mechanical properties all show a rich variation with mixture composition and particle size ratio, and can therefore be tuned by choosing certain mixtures. We identify two local minima in the critical volume fraction, both of which have low structural order; one minimum is close to the widely studied 50:50 mixture of particles with a ratio of radii of 1:1.4. We also identify a region at low size ratios characterized by increased structural order, with a corresponding enhancement in the stiffness.

Samenvatting

Dit proefschrift beschrijft de mechanische eigenschappen van amorfe vaste stoffen zoals schuim, emulsies en granulaire materialen. Elk van deze systemen bestaat uit "deeltjes" (bellen, druppels, korrels) in een dichte, ongeordende structuur. Bij compressie van een dergelijk systeem worden er uiteindelijk voldoende contacten tussen deeltjes gevormd om een belasting (waaronder bijvoorbeeld ook schuifspanning) te dragen. Op precies dat moment kunnen we zeggen dat het systeem is vastgelopen of geblokkeerd (in het Engels: "jammed"). Een grote theoretische uitdaging is het beschrijven van materiaaleigenschappen in de buurt van deze niet-evenwicht faseovergang.

Jamming is uitgebreid bestudeerd voor één specifiek model, namelijk niet-Brownse pakkingen van zachte wrijvingsloze schijven of bollen. Deze deeltjes stoten elkaar af wanneer ze overlappen en anders zijn er geen interacties. De pakking bestaat uit twee verschillende deeltjesgroottes om kristallisatie te voorkomen. Om dit te bereiken zijn de concentratie en diameterverhouding van de twee soorten deeltjes vastgelegd op specifieke waarden. Er is weinig bekend over de eigenschappen van "jammed systems" die ontstaan wanneer deze eisen ten aanzien van de deeltjes worden losgelaten. Dit is een aanzienlijke kennislacune omdat bellen, druppeltjes en korrels vaak een zekere mate van aantrekking tot hun buren ervaren (bijvoorbeeld als gevolg van capillaire bruggen of depletie interacties), en de deeltjesgrootteverdeling in de praktijk aanzienlijk kan variëren. Het doel van dit proefschrift is om te bepalen of en hoe het zachte bolmodel jamming ondergaat (i) bij het introduceren van verschillende mate van aantrekking tussen de deeltjes, en (ii) bij het variëren van de grootte en molverhouding van deeltjes in een bidisperse pakking.

Aantrekking.— Allereerst bestuderen we hoe zachte deeltjes met een attractieve schil een stijf materiaal kunnen vormen. Door de percolatie van starre clusters van deeltjes te analyseren wordt bewijs geleverd voor twee verschillende scenario's voor jamming. Systemen van sterk aantrekkende deeltjes ondergaan een continue transitie waarin starre clusters groeien die uiteindelijk bij een kritische pakkingsfractie divergeren in grootte. Puur repulsieve en zwak aantrekkende systemen ondergaan jamming via een eerste orde overgang, zonder groeiende clustergrootte. We laten zien dat het scenario van zwakke aantrekkingskrachten een zogenaamd finite-size effect is, zodat voor elke aantrekkingskracht die niet nul is, een voldoende groot systeem in de universaliteitsklasse van sterk aantrekkende deeltjes valt. We verwachten dan ook dat jamming van deeltjes die elkaar aantrekken generiek zal zijn in het laboratorium en in de natuur. Ten tweede onderzoeken we de elasticiteit van de vaste fase bestaande uit sterk aantrekkende deeltjes. Door het jamming punt als een kritisch punt te beschouwen, gebruiken we een zogenaamde "critical scaling" analyse om de afschuifmodulus, bulkmodulus en coördinatiegetal van marginale vaste stoffen dicht bij het jamming punt te bepalen. We vinden dat elke observeerbare grootheid niet alleen kwantitatief maar ook kwalitatief verschilt van het geval van puur repulsieve deeltjes.

Grootte- en molverhouding.— We brengen systematisch de jamming overgang van 2D bidisperse mengsels van schijven in de harde deeltjeslimiet in kaart. De kritische volumefractie en verschillende structurele en mechanische eigenschappen vertonen alle-maal een rijke variatie met de mengselsamenstelling en deeltjesgrootteverhouding. Deze kunnen daarom worden aangepast door bepaalde mengsels te kiezen. We identificeren twee lokale minima in de kritische volumefractie, die beide een lage structurele orde hebben; één minimum ligt dicht bij het veel bestudeerde 50:50 mengsel van deeltjes met een diameterverhouding van 1:1.4. We identificeren ook een gebied met kleine groot-teverhoudingen dat wordt gekenmerkt door een verhoogde structurele orde, met een overeenkomstige verbetering van de stijfheid van het materiaal.

1

INTRODUCTION

1

1.1. JAMMING

E MULSIONS, foams, and other forms of soft matter can either flow like a fluid or sustain deformations like a solid, depending on their density. This difference is the consequence of a non-equilibrium phase transition known as jamming. A jamming transition occurs when a collection of non-Brownian "particles" (droplets, bubbles, etc.) interacting via finite-ranged forces becomes rigid [1, 2]. *Rigidity* refers to a solid-like state that is capable of resisting small distortions elastically; in the language of continuum mechanics, the system has a shear modulus. Rigidity contrasts with *floppiness*, which refers to a fluid-like state that can accommodate shear through collective motions that do not cost energy; it therefore has zero shear modulus [3–6]. The horizontal axis of Fig. 1.1 represents a simple phase-diagram for the jamming transition. The figure is a schematic plot of the shear modulus G versus the particles' packing fraction ϕ. The jammed phase ($G > 0$) is separated from the unjammed phase ($G = 0$) by a jamming point at a critical value of the packing fraction, ϕ_c.
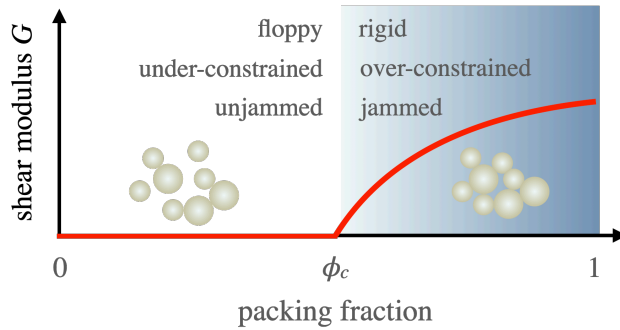

Figure 1.1: Schematic jamming phase diagram, based on ideas proposed in [7]. The shear modulus G is shown on the vertical axis. Its value is non-zero in the jammed phase nad zero in the unjammed phase. Packing fraction ϕ is defined as the ratio of total particle volume to system volume; respectively, particle and system area in 2D.

Jamming is not an equilibrium thermodynamic phase transition like freezing/melting, and therefore cannot be understood through the traditional toolkit of statistical mechanics. Instead, it is a constraint satisfaction problem controlled by the relative abundance of degrees of freedom (the individual particles' motions) and constraints on motion (the contacts between interacting particles). In an approximate (mean field) sense [8, 9], the system is floppy/unjammed when the it is under-constrained (degrees of freedom are more numerous than constraints); and the system is rigid/jammed when the it is over-constrained (there are more than enough contacts to constrain all particle motions). The jamming point at ϕ_c is a marginal state where degrees of freedom and constraints precisely balance. A more rigorous definition of jamming (one which accounts for spatial heterogeneity in the contact network) will be presented in Chapter 2 using the language of percolation theory.

Despite the transition's non-equilibrium character, systems close to the jamming point display behavior similar to equilibrium systems near a critical point. For example, the shear modulus in Fig. 1.1 scales as a power law in the distance to the jamming point, $\phi - \phi_c$. An overarching goal of the research literature on the jamming transition, including this thesis, is to identify, characterize, and explain the origins of these critical properties.

1.2. SYSTEMS WHERE JAMMING IS RELEVANT

NUMEROUS systems exist in a jammed phase or undergo an (un)jamming transition. These systems, and the processes in which they are found, provide a practical motivation for studying jamming. To understand the rheological behavior of these systems, knowledge of physics in the vicinity of the jamming transition is essential. Here we give several examples.

- *Aqueous foams* — Aqueous foams are formed from a discontinuous gaseous phase dispersed in a continuous liquid phase. The gas forms bubbles which favor a spherical shape, to minimize the energetic penalty of surface tension. A familiar example from everyday life is shaving foam, where typical bubble sizes range from tens of micrometers to millimeters. Foams also have medical applications, e.g. in sclerotherapy, where the foam is injected in a blood vessel to remove a clot, see Fig. 1.2 for a schematic from Ref. [10]. Note that the term "foam" can also be used for solid foams, such as the sort found in bicycle helmets. Solid foams are not the topic of this thesis.

- *Emulsions* — Emulsions are quite similar to aqueous foams, with the exception that the discontinuous phase is also a liquid (which is immiscible in the continuous phase). Perhaps the most familiar example of an emulsion is oil-in-water. The droplets in emulsions are comparable in size to foam bubbles. Emulsions appear in a number of industrial settings, including enhanced oil recovery, fracking, and food products such as sauces. One specific food-related challenge is illustrated in Fig. 1.3 from Ref. [11]. Consumer preferences are often influenced by the so-called "mouthfeel" of products, which ultimately arise from the rheological properties of food. Because systems near jamming are highly sensitive to constitutive properties such as packing fraction, there is the potential to tune the flow behavior of a product, and thereby positively influence consumer satisfaction.

- *Pastes and granular media* — Pastes are formed from dense dispersions of solid particles in a solvent, for example toothpaste. Granular materials such as sand are also dense packings of particles, albeit usually in air. Solid particles can vary significantly in size, from micrometers in colloids to centimeters in granular media. In both pastes and granular media, it is possible for the particles to stick together due to the presence of liquid bridges localized near the contacts. This phenomenon is the reason a sand castle does not fall down. Packings can be stabilized by liquid bridges (see Fig. 1.4) to create weakly jammed states, and thereby offer a route to tailored material properties. For example, recent work in Ref. [12] showed that by placing a polymer in the liquid, the system can be formed, malleably shaped, and thereafter set by curing the polymer.
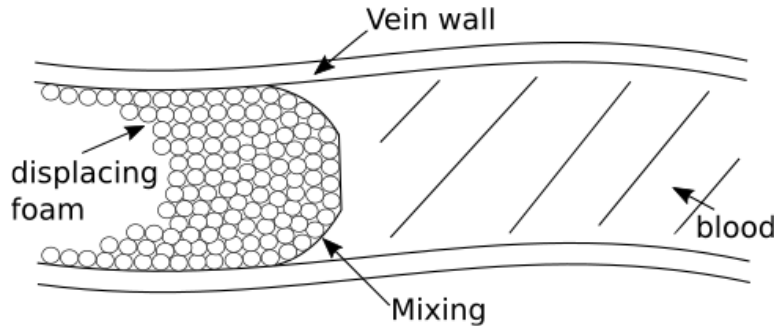
Figure 1.2: From Ref. [10]: foam displacing the blood in a vein as part of a treatment for blood clots. The jammed phase of bubbles displaces the blood in malformed vessels while carrying the sclerosant drug that causes the vessel walls to to thicken and eventually form into scar tissue. By displacing the blood the drug can be delivered more precisely.

(a) One of the bouillons considered in [11].
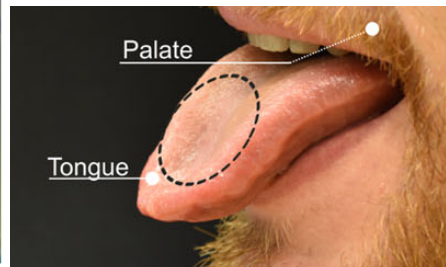
(b) The tongue and palate are involved in assessing the rheological properties that make up the mouthfeel.

Figure 1.3: From Ref. [11]: Rheological properties of emulsions determine the mouthfeel of food products.
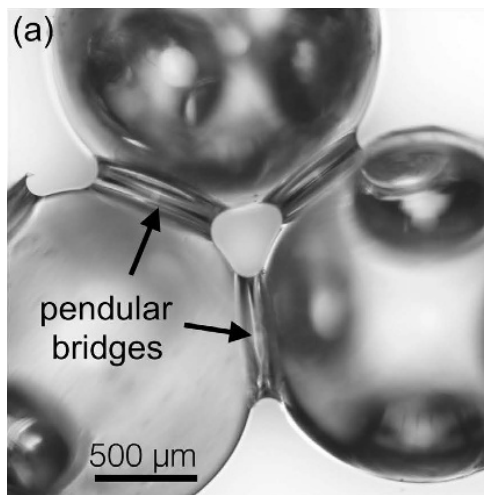
Figure 1.4: From Ref. [12]: polymer bridges formed between beads. These bridges can be cured and subsequently stabilized, tuning the material properties.

For an extended discussion of jamming and applications of jammed media, the reader is referred to Ref. [13]

1.3. MODELS AND SIMULATIONS

To understand a physical phenomenon, it is often useful to study it in the context of a minimal model. By "minimal" we mean a model in which details that are not essential to the phenomenon in question are stripped out. A textbook example of a minimal model is the Ising model for the transition from a non-magnetic to a ferromagnetic state. A large majority of the research on jamming has sought to understand generic ("universal") properties of systems near the transition point, rather than developing models that reproduce the properties of specific materials in detail.

In the jamming literature, researchers have focused on a minimal model known as "the soft sphere model" [1] or, alternatively, "the bubble model" [14]. This model is focused on the particle scale, such as a foam bubble, emulsion droplet, or sand grain. Each particle is assigned its own degrees of freedom (in this case, position). Physics on shorter length scales, such as intermolecular interactions, is incorporated via effective interactions between neighboring particles. For a discussion of other models of jammed systems, the reader is referred to [2].

The key ingredients of the soft sphere model are as follows:

- Particles are modeled as spheres in 3D or disks in 2D.

- Particles are much larger than the size of a molecule, and therefore experience negligible thermal fluctuations. In other words, they are "athermal" or "non-Brownian".

- Particles are "soft", which means they are allowed to interpenetrate. This "overlap" between particles generates a restoring force that pushes them apart. One can

1

think of overlap as an effective way to incorporate deformations of particles due to surface tension and/or bulk elasticity.

• All forces between particles have a finite range. In practice this means that particles interact when they are physically in contact, otherwise not.

• Static friction is neglected. This approximation is mild in the case of emulsions and foams, but stronger for granular media.

• Gravity is neglected. This is necessary to achieve a homogeneous system.

• The system nearly always consists of a 50:50 mixture of large and small particles with a diameter ratio of 1.4:1. This is chosen for two reasons. First, the physical systems we are motivated to study are polydisperse and do not crystallize. This bidisperse distribution also does not crystallize. Second, using the same size distribution as other studies facilitates comparison of results.

The soft sphere model lends itself to computer simulations of interacting particles. Conventionally, jammed states are prepared in the following way:

• The particles are confined to a unit cell of fixed volume (or pressure). The unit cell has periodic boundary conditions to reduce finite size effects and preserve homogeneity.

• Particles are seeded in the unit cell by a random point process at a target value of the packing fraction ϕ, i.e. the total volume of the particles divided by the volume of the cell. In 2D the term "volume" should be understood to refer to area.

• The system is brought to the nearest local minimum of its potential energy landscape via an instantaneous quench. One can think of this as going instantaneously from a state at infinite temperature (the point process) to zero temperature (the energy minimized jammed state).

• Properties of the jammed system are calculated from averages over ensembles of states generated in the same way, e.g. at the same packing fraction.

Unlike thermal systems describable with equilibrium statistical mechanics, jammed systems are out of (thermal) equilibrium and their properties can be protocol dependent. Following a standard protocol facilitates comparison of results across studies.

1.4. OPEN QUESTIONS ADDRESSED IN THIS THESIS

THIS thesis addresses two major open questions in the scientific literature on jamming using the soft sphere model as our research tool.

• *Attractive interactions*— Bubbles, droplets, and grains routinely experience some degree of attraction to their neighbors. This can have different, system-specific origins. Examples include depletion interactions due to surfactants in an emulsion, finite contact angles between bubbles in a foam, or liquid bridges in capillary

suspensions and wet granular media. Regardless of their origin, the key point is that particles in these systems do attract their neighbors over short distances (compared to the particle size). The standard soft sphere model, however, does not account for these attractions: particles are assumed to have purely repulsive interactions. How attractions affect the jamming transition is an open question.

- *Bidisperse mixtures*— As noted above, studies of jamming nearly always employ a standard mixture of large and small particles to avoid crystallization. Physical systems, however, can display a broad array of size distributions. The extent the properties of the "standard" mixture are generic is largely unexplored. A natural generalization of the standard model, and a step closer to reality, is to vary the size and number ratio of the particles in the mixture and investigate its effect on the jamming transition.

1.5. STRUCTURE OF THE THESIS

I N this thesis we go beyond the standard soft sphere model to investigate the role of attraction and bidispersity on the jamming transition. The work is organized as follows.

In Chapter 2 jamming in attractive systems is investigated as a rigidity percolation problem. By systematically varying the strength of attraction between particles while monitoring the statistics of rigid clusters, we determine how attraction alters the location and character of the jamming point. We will show that attractive jamming is a second order phase transition, in contrast to repulsive jamming, which is massively first order. The crossover between first and second order transitions occurs at a characteristic attraction strength that vanishes in the limit of large systems.

Whereas in Chapter 2 we focus on the jamming point itself, in Chapter 3 we systematically vary the distance to the jamming point in attractive systems. We find that the elasticity of attractive jammed solids is controlled by proximity to the transition, and identify novel constitutive relations that describe the elastic moduli. Unlike repulsive systems, we find that both the shear and bulk modulus vanish continuously at the transition point in the same way.

Finally, in Chapter 4, we explore the character of bidisperse mixtures near jamming. By varying the number and size ratio of two species of particles, we show that the location of the jamming transition can be shifted. We characterize the space of transitions by degree of crystallinity and find that the standard repulsive soft sphere model lies within a basin of qualitatively similar states.

2

RIGIDITY IN ATTRACTIVE SOFT DISK PACKINGS

While the large majority of theoretical and numerical studies of the jamming transition consider athermal packings of purely repulsive spheres, real complex fluids and soft solids generically display attraction between particles. By studying the statistics of rigid clusters in simulations of soft particles with an attractive shell, we present evidence for two distinct jamming scenarios. Strongly attractive systems undergo a continuous transition in which rigid clusters grow and ultimately diverge in size at a critical packing fraction. Purely repulsive and weakly attractive systems jam via a first order transition, with no growing cluster size. We further show that the weakly attractive scenario is a finite size effect, so that for any nonzero attraction strength, a sufficiently large system will fall in the strongly attractive universality class. We therefore expect attractive jamming to be generic in the laboratory and in nature.
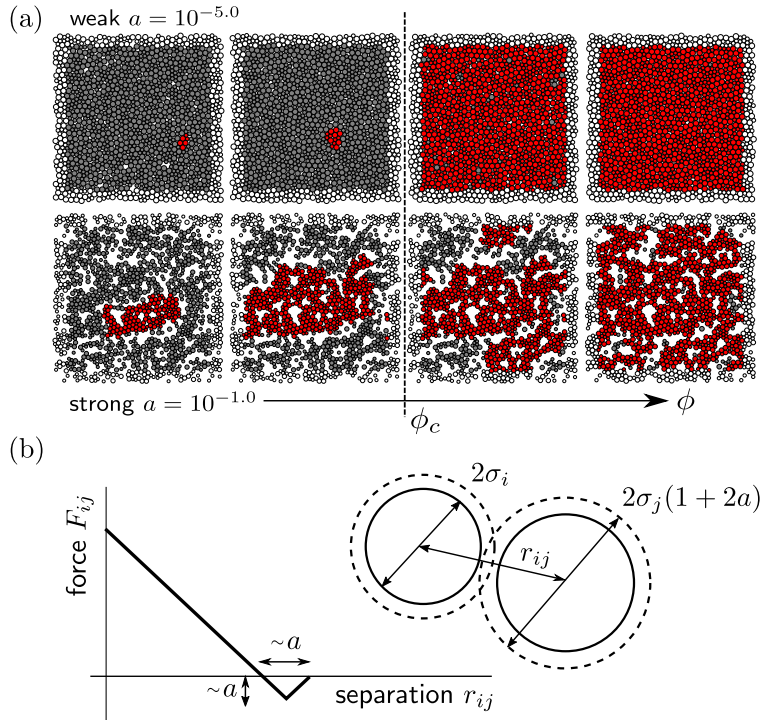
Figure 2.1: (a) Packings with weak and strong attraction for packing fractions ϕ near the point ϕ_c where they jam. Particles in red form the largest rigid cluster. (b) Contact force law for a pair of particles with an attractive shell.

Numerous complex fluids, including emulsions, foams, pastes, powders, sand, and blood, can jam into soft amorphous solids under increasing packing fraction [2, 15]. In recent years, enormous progress towards a fundamental understanding of jammed matter has been driven by theoretical and numerical studies of dense systems of athermal spheres interacting via purely repulsive contact forces. There is now general agreement on how the structure and mechanics of repulsive soft spheres are governed by proximity to the jamming transition at a critical packing fraction ϕ_c – see e.g. [1, 14, 16–23] for a partial list. This line of study implicitly builds on the assumption that repulsive particles yield broad or even universal insights into the marginally jammed state. Nevertheless, purely repulsive interactions are not generic in the laboratory or in nature. While stickiness has various origins (e.g. van der Waals forces [24], depletion effects [25, 26], wetting effects [27–29], interface deformation [30, 31], critical Casimir forces [32], etc.), particles typically attract their neighbors, and pure repulsion can only be realized with careful tuning, if at all. The few existing studies of jamming with attraction reveal significant differences, including a gel-like structure with large voids [33, 34] and shear banding [35–38]. Most remarkably, Lois et al. [39] showed that strongly attractive soft spheres belong to a new universality class, distinct from both repulsive jamming and rigidity percolation on generic lattices [40, 41]. But it remains unclear when repulsive jamming gives way to

attractive jamming – one cannot currently predict whether a given experimental system falls into the repulsive or attractive jamming class.

In this Chapter, we demonstrate the striking influence of attraction on the growth of rigid clusters, illustrated in Fig. 2.1. A cluster is rigid if, when removed from the packing, its only zero frequency vibrational modes are rigid body motions. A system is jammed if it contains a spanning rigid cluster [3]. Fig. 2.1a depicts disk packings with "weak" (top row) and "strong" (bottom row) attraction; they differ in the thickness of an attractive shell (panel b). The largest rigid cluster in each packing is shaded red. For weak attraction, the largest cluster contains just a few particles, and a spanning cluster appears suddenly at ϕ_c. This scenario resembles the first order transition observed in repulsive systems [40, 41], suggesting attraction acts as a small perturbation. In sharp contrast, clusters in strongly attractive systems grow in size before spanning at ϕ_c, reminiscent of a continuous phase transition with a diverging length scale.

What distinguishes repulsive, weakly attractive, and strongly attractive jamming? Here we use rigid cluster decomposition to identify the attractive jamming point and to quantitatively assess the order of the jamming transition. Then, by systematically varying attraction and particle number, we determine when weakly attractive jamming ends and strongly attractive jamming begins. Our central result is that attraction is never weak in the limit of asymptotically large system sizes – large systems are either purely repulsive or strongly attractive, and any amount of attraction places a system in the universality class of strongly attractive jamming.

Methods and protocol.— We consider athermal systems of N disks in a 50:50 bidisperse mixture with size ratio 1.4:1 to avoid crystallization [1, 42] and periodic boundary conditions to eliminate wall effects. Unless stated otherwise we choose $N = 1024$. Athermal attractive particles are strongly protocol-dependent, because contacts can only break or form through external excitation. We employ a standard preparation protocol in which particles are initially placed at random, followed by a quench at fixed ϕ to a local energy minimum using a nonlinear conjugate gradient method [1]. The conjugate gradient method is discussed further in Appendix 2.4. Note that, unlike repulsive jamming, the the jamming point cannot be identified with zero pressure, as tensile states are accessible [33].

We adopt the conventions of prior work [34–39] and model sticky particles with a repulsive core and attractive shell that experience a central force

$$F_{ij} = \begin{cases} k\delta_{ij} & \delta_{ij} \geq -\sigma_{ij}a \\ -k(\delta_{ij} + 2a\sigma_{ij}) & -\sigma_{ij}a > \delta_{ij} \geq -2\sigma_{ij}a \\ 0 & \delta_{ij} < -2\sigma_{ij}a \end{cases} \qquad (2.1)$$

between particles i and j (see Fig. 2.1b). The spring constant k characterizes repulsion, while the dimensionless attraction strength a sets the attractive shell thickness and the maximal tensile force. $\delta_{ij} = \sigma_{ij} - r_{ij}$ is the overlap between two particles and σ_{ij} is the sum of the radii of their cores. The packing fraction ϕ is calculated from the particles' cores. Including the attractive shell would increase ϕ by a factor $1 + 4a$, to leading order in a.

The pebble game algorithm [3] efficiently and unambiguously identifies all rigid clusters in two spatial dimensions, dictating our choice to simulate disk packings. The

2
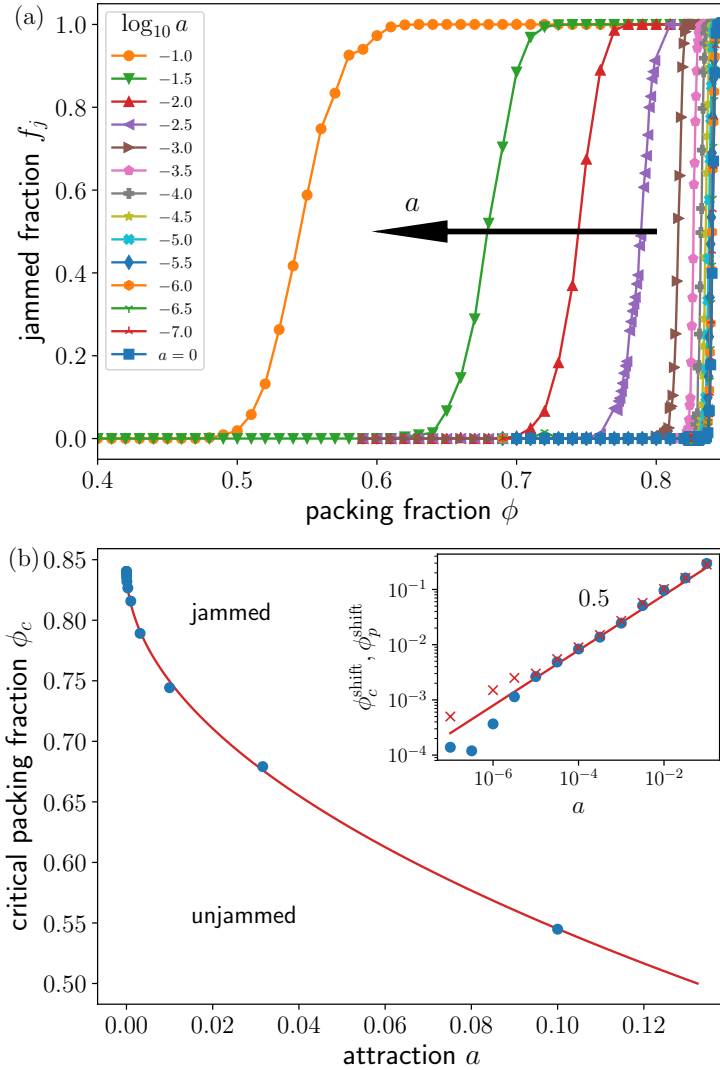
Figure 2.2: (a) Fraction of jammed states f_j versus packing fraction ϕ for varying attraction strength a and $N = 1024$. (b) Attractive jamming phase diagram. (inset) Scaling of the shift in $\phi_c(a)$ (filled circles) and $\phi_p(a)$ (crosses) with a.

algorithm outputs disjoint sets of bonds (i.e. clusters) whose bonds are rigid with respect to each other. Details are found in Appendix 2.5. Accurate contact identification is essential for rigid cluster decomposition. Unlike repulsive particles, identifying contacts with attraction is straightforward because particles tend to sit near the first zero of F_{ij} (i.e. the minimum of their pair potential).

2.1. JAMMING PHASE DIAGRAM.

As we are considering physics near jamming, we first determine the critical packing fraction ϕ_c as a function of attraction strength.

For finite particle number N, the jamming transition is "blurred" by finite size effects, as seen in a plot of the fraction f_j of jammed packings in ensembles prepared at a given ϕ (Fig. 2.2a). The purely repulsive packings show a rapid increase of f_j at a packing fraction near 0.84. As attraction strength a increases, the rise in f_j shifts to lower ϕ and also becomes more gradual. We will first focus on the shift and then on the widening of f_j.

We associate a critical packing fraction $\phi_c(a, N)$ with the value of ϕ where $f_j(\phi, a, N) = \Delta$ with $\Delta = 0.5$. The shift of the transition is then defined with respect to the purely repulsive jamming point, *i.e.* $\phi_c^{\text{shift}}(a, N) = \phi_c(0, N) - \phi_c(a, N)$. Henceforth we drop the N dependence of $\phi_c(a)$ whenever $N = 1024$. We have verified that the scaling of ϕ_c^{shift} is insensitive to variations in Δ around 0.5. In Fig. 2.2b we see how $\phi_c(a)$ decreases with increasing a, dividing the diagram into unjammed and jammed phases. The shift is plotted in the inset of Fig. 2.2b (filled circles). We find power law scaling that is well described by $\phi_c^{\text{shift}} \sim a^{0.5}$. Note that the excess volume occupied by attractive shells, which scales linearly in a, cannot trivially account for this rapid decrease.

We now ask if the jamming transition is sharp in the large system size limit. We focus on "weak" ($a = 10^{-5.0}$) and "strong" ($a = 10^{-1.0}$) attraction, plotted in Fig. 2.3a and b, respectively. For $N = 128 \ldots 2048$, f_j can be collapsed by plotting versus $\Delta\phi N^{\alpha}$, where $\Delta\phi = \phi - \phi_c(a, N)$ (unscaled data are shown in the Supplementary Material). We observe data collapse for positive values of the exponent α, hence f_j approaches a step function as $N \to \infty$ and the transition is indeed sharp. However, the value of α providing the best collapse for the plotted range of N is different for weak and strong attraction – $\alpha \approx 0.4$ versus 0.2, respectively. This is the first indication in our data of a distinction between weak and strong attraction. Below we present evidence for a crossover $a^* \sim 1/N$ between weak and strong attraction. Hence for asymptotically large N and nonzero attraction strength, we expect (i) f_j versus $\Delta\phi N^{\alpha}$ to collapse for the same $\alpha \approx 0.2$, and (ii) the cluster size distribution $P(N_c, \phi_c)$ to be gapless.

2.2. ORDER OF THE TRANSITION.

The growth of rigid clusters illustrated in Fig. 1 suggests that jamming is a continuous transition in strongly attractive systems, and a first order transition in weakly attractive (or purely repulsive) systems. We now make these observations quantitative by studying the probability $P(s; a, \phi)$ a given cluster has s particles. From percolation theory we expect $P(s; a, \phi_c)$ to be gapped in systems with a first-order transition, and to be gapless for a continuous transition [41, 43].

The cluster size distribution at ϕ_c is plotted in Fig. 2.4a and b for weak and strong attraction, respectively. For weak attraction there is a gap between small clusters of tens of particles or less, and large clusters that contain nearly all particles in the packing, indicating a first order transition. We have verified that the large cluster peak is solely populated by jammed packings, while small clusters occur in both unjammed and jammed packings.

The cluster size distribution for strongly attractive packings in Fig. 2.4b shows no gap, indicating a continuous transition. We have verified that both jammed and unjammed

2
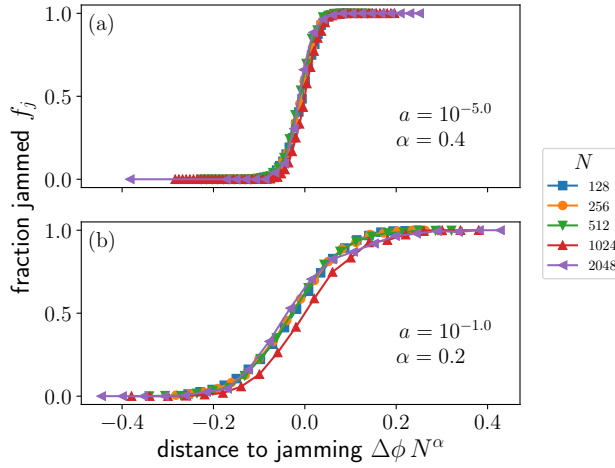
Figure 2.3: Data collapse of the fraction of jammed states for varying particle number N in (a) weakly attractive and (b) strongly attractive systems.
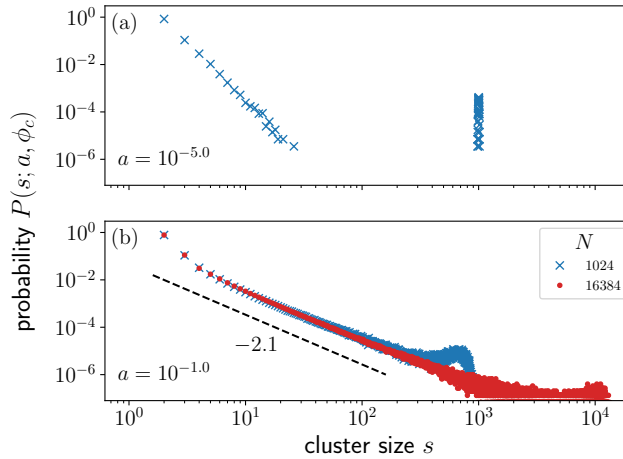
Figure 2.4: Cluster size probability distribution for (a) weakly attractive and (b) strongly attractive systems.

packings populate the full range of cluster sizes. The distribution has a power law tail $P \sim s^{-\tau}$ that extends to cluster sizes of order N. To better estimate the exponent τ, we plot the same distribution for a system of $N = 16384$ particles to find $\tau \approx 2.1$ (dashed line). The small peak for s close to $N = 1024$ in the smaller systems is due to finite size effects, including the finite width of f_j. Note that the peak is reduced for larger N, while the distribution remains gapless.
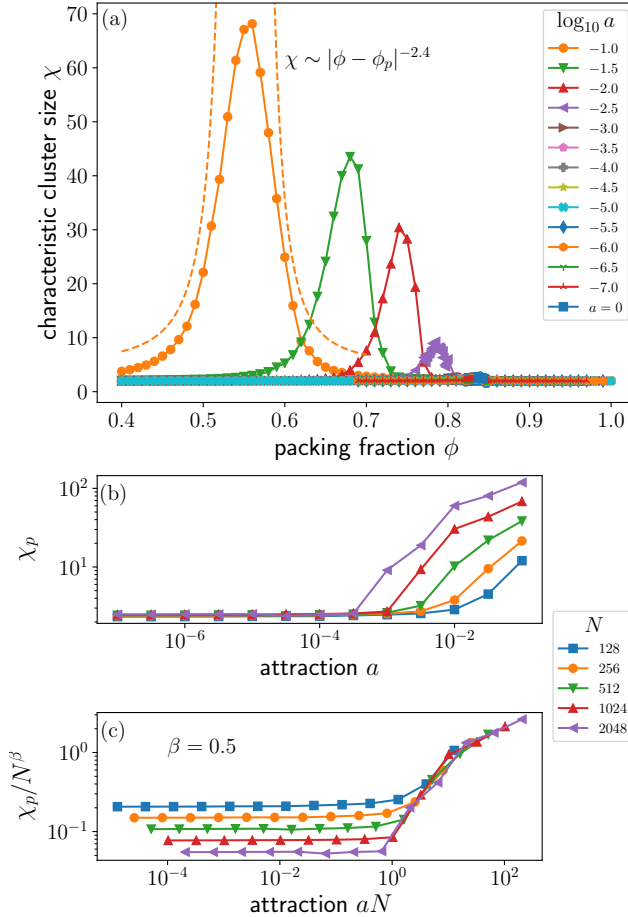
Figure 2.5: (a) Cluster size dependence on packing fraction. Dashed line shows inferred divergence of infinite system (offset vertically). (b) Evolution of the peak cluster size with attraction strength for varying particle number N. (c) Rescaled data from (b).

2.3. GROWING CLUSTER SIZE.

Having addressed statistics at ϕ_c, we now probe cluster size as ϕ is swept through the jamming transition. Our results will further validate the first order and continuous characterization of weakly and strongly attractive jamming, respectively. Of equal importance, we will also identify the characteristic attraction strength a^* separating weak and strong attraction.

For a continuous percolation transition, one expects to find a typical cluster size that diverges at the transition, while the same quantity should remain finite at a first order transition [43]. To quantify cluster sizes on either side of jamming, we introduce the probability $n(s; a, \phi)$ that a given non-spanning cluster has s particles and calculate the

expected cluster size of a randomly selected particle outside the spanning cluster,

$$\chi(a,\phi) = \frac{\sum_s s^2 \, n(s; a, \phi)}{\sum_s s \, n(s; a, \phi)} \, . \tag{2.2}$$

In Fig. 2.5a, χ is plotted versus packing fraction for varying attraction strength. While data for the lowest values of a show no dramatic features, for the strongest attraction strengths there is a substantial increase in χ near ϕ_c. To quantify these observations, we extract the height χ_p and position ϕ_p of the peak in χ. From ϕ_p we calculate the shift $\phi_p^{\text{shift}}(a) = \phi_c(0) - \phi_p(a)$. We find excellent agreement between the position of the peak and ϕ_c determined from Fig. 2.2a, as demonstrated in the inset of Fig. 2.2b. We conclude that the peak in χ coincides with the jamming point.

We now ask if the peak cluster size diverges as $N \to \infty$. Fig. 2.5b shows χ_p as a function of a for varying N. At low a, typical clusters consist of a few particles. There is no trend with N, suggesting that χ_p remains finite. For strong attraction χ_p grows with N, and the attraction a^* where χ_p starts to grow is lower in larger systems. To gain insight into these effects, in Fig. 2.5c we replot the data as χ_p/N^β versus aN. We observe collapse to a master curve when $aN \gtrsim 1$ and $\beta \approx 0.5$. As β is positive and the master curve increases with aN, we infer that χ_p diverges in the large system limit – there is indeed a diverging cluster size, consistent with a continuous transition. For the largest a, the cluster size diverges as $\chi \sim 1/|\phi - \phi_p|^{2.4}$ (vertically offset dashed curve in Fig. 2.5a; log-log plot in the Supplementary Material).

A key finding is that the rescaled attraction strength aN in Fig. 2.5c implies the existence of a characteristic scale $a^* \sim 1/N$. Systems with a above (below) a^* jam according to the strongly (weakly) attractive scenario. Hence any nonzero attraction strength satisfies $a > a^*$ in a sufficiently large system, and in the $N \to \infty$ limit *all* attractive systems jam according to the strongly attractive scenario. In other words, attraction is never a weak perturbation to repulsive jamming.

Discussion.— We have demonstrated that rigid clusters form a jammed phase in purely repulsive and weakly attractive systems via a first order transition in which the spanning cluster appears suddenly at the critical packing fraction. In sharp contrast, strongly attractive systems jam via a continuous transition with a typical cluster size that diverges at ϕ_c. The first order transition for weak attraction is a finite size effect, and in thermodynamically large systems the jamming universality class is either purely repulsive ($a = 0$) or attractive ($a > 0$). As attraction is generic in experimental systems, we predict that they jam according to the attractive scenario.

Some of our results can be compared to work by Zheng et al. [34] and Lois et al. [39], with the caveat that preparation protocols differ. Zheng et al. observed a critical packing fraction shift $\phi_c^{\text{shift}} \sim a^{0.3}$, extracted from four values of a over three decades; we find an exponent 0.5 with finer sampling. Lois et al. [39] report data for just one attraction strength comparable to our $a = 10^{-2}$. They found the fraction of jammed states collapses with $\alpha \approx 0.16$, and a cluster size exponent $\tau \approx 2.1$, in accord with our $\alpha \approx 0.2$ and $\tau \approx 2.1$. Henkes et al. recently studied rigid clusters in frictional shear flow [41]. Despite the obvious differences between friction and attraction, they also found a continuous transition at nonzero friction.

There are several likely directions for future work. Foremost, it remains to determine

the influence of rigid clusters on mechanics, such as storage and loss moduli [6, 22, 23], yield stress [19, 36, 37, 44–47], nonlocal effects [48–50], and shear banding [36, 37, 51]. By varying the pair potential, once can also untangle the roles of the range and strength of the attractive interaction. The phase diagram for attractive glasses and gels has ϕ on one axis and the ratio of the attractive well depth U to the thermal scale $k_B T$ on the other. Jammed states at $T = 0$ sit deep in the glass/gel phase, hence one anticipates connections to vitrification or gelation as T increases [52–55].

2

2.4. APPENDIX: CONJUGATE GRADIENT MINIMIZATION

The conjugate gradient (CG) algorithm is originally designed for solving a linear system of equations. However, it can be adapted for nonlinear problems, and despite the lack of mathematical proof it turns out that it performs well in most cases. Descriptions of CG in its original linear variant or nonlinear variant can be found in [56–58]. Below we provide a short description of the general CG algorithm, before turning to the nonlinear extension required for soft sphere packings. Finally we will discuss some considerations on stopping criteria.

The goal is to minimize the energy $U(\mathbf{r})$ with the gradient $\nabla U(\mathbf{r}) = -\mathbf{f}(\mathbf{r})$. It is an iterative method, so we will find a sequence of vectors $\mathbf{r}_i$ which converges to a minimum in the energy. Let us for brevity denote $U_i = U(\mathbf{r}_i)$ and $\mathbf{f}_i = \mathbf{f}(\mathbf{r}_i)$. The idea behind CG is that the sequence $\mathbf{r}_i$ is obtained by following the gradient from the current position, but discarding any component of a direction that was searched in before. This yields an exact solution in at most Nd iterations if the problem were a set of linear equations. Since contacts are made and broken any potential will lead to a nonlinear energy landscape and the CG iterations needs to be restarted from time to time.

The initial position $\mathbf{r}_0$ is the randomly chosen positions of all particles. CG starts by greedily searching for a minimum in the direction of the gradient, *i.e.* $\mathbf{d}_0 = \mathbf{f}_0$. Then in each iteration the minimum along the current search direction is found and the search direction is updated based on the new position $\mathbf{r}_{i+1}$. Later we will spend some words on how the minimization along a direction is designed. The update to the new direction is done with the following scheme

$$
\begin{aligned}
\mathbf{r}_{i+1} &= \min\left(U(\mathbf{r})\,|\,\mathbf{r} = \mathbf{r}_i + t\mathbf{d}_i\right) \qquad t \in \mathbb{R} \\
\gamma_{i+1} &= \frac{(\mathbf{f}_{i+1} - \mathbf{f}_i)\mathbf{f}_{i+1}}{\mathbf{f}_i \mathbf{f}_i} \\
\mathbf{d}_{i+1} &= \mathbf{f}_{i+1} + \gamma_i \mathbf{d}_i
\end{aligned}
\tag{2.3}
$$

This process continues until a convergence criterion is met.

Numerical precision plays a role in the energy minimization at this point. Since there is a nonzero energy at the local minimum the change in energy suffers from catastrophic cancellation, as described earlier in this Chapter. Together with the rounding errors in cancellation in the overlap calculation this implies that there is a plateau of energy under which it is impossible to minimize, set by, but higher than, the precision of the floating point numbers. This problem is overcome by considering the gradient as a criterion instead. The directional gradient $\mathbf{f} \cdot \mathbf{d}_i$ will pass through zero at the minimum in the energy. The only limit to minimization here is the precision of the floating point numbers.

The nonlinear part of this CG algorithm is the search for a minimum along a direction $\mathbf{d}_i$. In this part most of the running time is spent, so it is useful to optimize this technique. In our implementation there is a series of estimates of where the minimum is of increasing complexity and increasing accuracy. They are tried in ascending order of complexity until they produce an estimated gradient at $\mathbf{r}_{i+1}$ that is close enough to the real gradient at that position. For all stages of estimation it is important to be aware that the nearest energy minimum needs to be found, otherwise it skips over some local minima. We will briefly describe these techniques here.

There is an inherent minimal scale to the energy landscape that is set by the type of potential and the number of particles. In practice it turns out that this scale sets the distance to the nearest energy minimum from the current r_i along d_i. The first estimate is therefore taking this step and evaluating whether the gradient there is close to zero.

If that fails the gradient is now evaluated at two points along the line and it is possible to a linear interpolation of where the nearest zero crossing of the gradient is. Again, if the gradient is not close to zero we continue with the next in line of complexity.

Similarly to the linear interpolation it is now possible to construct a parabolic approximation of the energy landscape with the third point at which the gradient is evaluated. If this also does not yield a gradient that is close to zero the algorithm defaults to a search algorithm.

The search algorithm takes steps in alternating directions until the gradient flips sign with decreasing step size. This is a very expensive, but when the initial step was not too large, guaranteed method of finding the nearest energy minimum. We would like to point out that this happens on average in just a handful of iterations, while the vast majority of iterations is solved with just a single gradient evaluation.

2

2.5. APPENDIX: RIGIDITY AND THE PEBBLE GAME

The pebble game is an algorithm that finds rigid clusters in planar graphs of rigid bars. In a packing with a purely repulsive pair potential, contact counting arguments can be made about rigidity and distance to jamming [2]. When there are for example tensile forces between particles this is not sufficient and we need a local version of contact counting. The pebble game developed in [3] provides such a criterion. With the rigid clusters in a packing we can formulate a criterion for jamming in these attractive packings.

We will start with some simple examples to build up some intuition. Then, in steps, we will formalize it until an algorithm for finding rigid clusters drops out.

For a first example we consider a simple triangle, see Fig. Figure 2.6a. Without the connections as constraints the three nodes can each move freely in the two-dimensional space, so each of them has two degrees of freedom. The total of six degrees of freedom are represented by the two circular pebbles on each node.

(a) Degrees of freedom of each node.   (b) One degree of freedom constrained by an edge.   (c) Three degrees of freedom left unconstrained: rigid body motions.
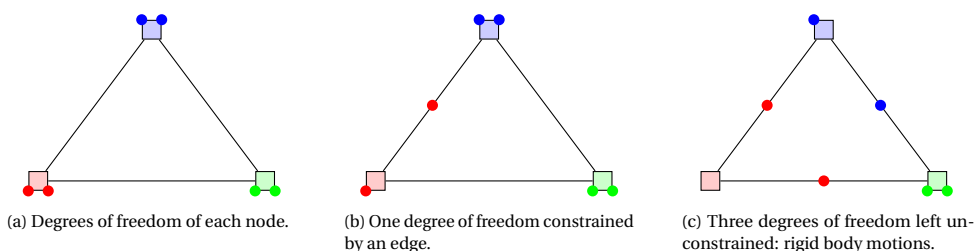
Figure 2.6: The basic idea of constraining degrees of freedom by edges illustrated on a triangle.

Every edge that is connected to a node constrains one degree of freedom, as the two nodes that are connected now need to be at a fixed distance from each other. This is represented by moving a pebble onto that edge, as in Fig. 2.6b. The degree of freedom is now constrained by that edge and does not represent a way in which the network can move any more. Degrees of freedom of a certain node can only be constrained by edges that are incident on that node. An edge at the other end of the network does not influence the degrees of freedom of that node directly. This is represented by the matching color of nodes and pebbles.

By placing pebbles onto the other two edges we could end up in the situation of Fig. 2.6c. Now all edges are covered by a pebble, so all the ways in which edges constrain the motion of the network are taken away from the degrees of freedom on the nodes. There are three degrees of freedom left on the nodes: 1 blue and 2 green. This means the network can move in three ways, two rigid body translational modes and one rigid body rotational mode. Any network, whether rigid or floppy, will always have at least these three degrees of freedom.

Now consider a slightly larger network that contains a floppy mode. The square in Fig. 2.7a again has two pebbles on each node at the start. In the same way as before each edge constrains one degree of freedom, represented by putting one degree of freedom onto that edge. This might result in the situation in Fig. 2.7b where the red and green node have three degrees of freedom representing the three rigid body motions of this part of the network. In this example, however, there is another degree of freedom on the yellow

node. This network has one more way of deforming than the three rigid body motions. This extra floppy mode is illustrated in Fig. 2.7c and is known as shearing the square.

(a) The initial state with all degrees of freedom on the nodes.

(b) All edges are covered with degrees of freedom: four degrees of freedom are still unconstrained.

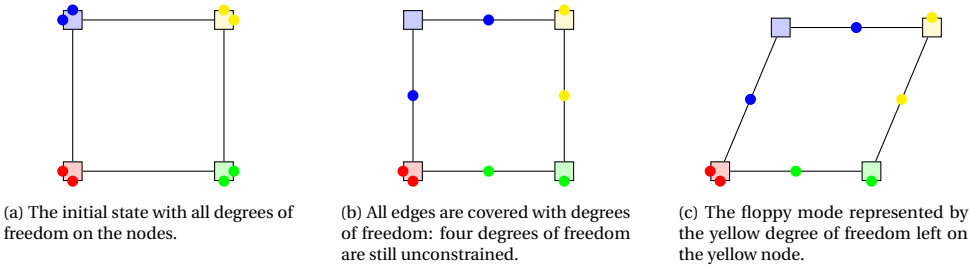(c) The floppy mode represented by the yellow degree of freedom left on the yellow node.

Figure 2.7: The pebble game applied to a simple network with a floppy mode.

The square in Fig. 2.7 can be made rigid by adding a new node and some more edges as in Fig. 2.8a. If all edges are now covered with pebbles as before only two degrees of freedom are left on nodes, see Fig. 2.8b. However, such a state is not possible as any network has three degrees of freedom for the rigid body motions. This must mean that a degree of freedom was constrained with by redundant edge.

In the particular distribution of pebbles in this example it can be seen that the edge between the red and magenta node is not required. Even if this edge, that is now covered by a red pebble, is left out the red node is rigidly attached to the rest of the network. In Fig. 2.8c we see the distribution of pebbles after correcting the mistake. The dashed edge does not add any new constraint on top of the other edges, so it should not be covered by a pebble.

(a) The initial state with all degrees of freedom on the nodes.

(b) All edges are naively covered by a pebble, which results in the impossible state of two free degrees of freedom.

(c) The dashed edge is redundant and should not be covered by a degree of freedom.
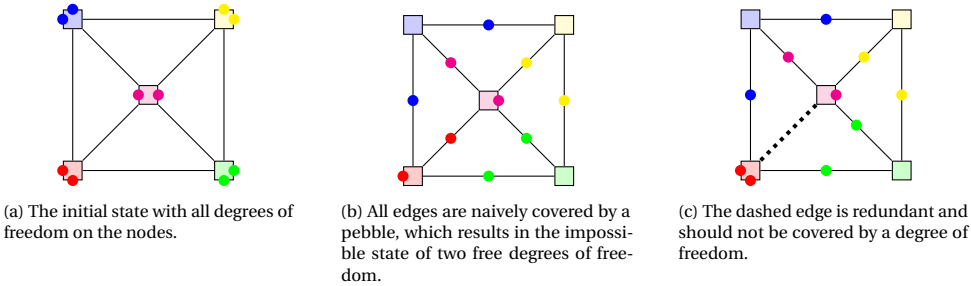
Figure 2.8: The pebble game applied to a simple over-constrained network.

We will now discuss how to detect redundant edges in a network in general. In order to detect this we need to introduce a swapping operation. The particular distribution pebbles on the edges is not unique; there is some freedom to choose which pebbles cover which edges. This allows the unconstrained degrees of freedom to move around, see the illustration in Fig. 2.9a. Even though degrees of freedom are localized around their corresponding node a 'virtual' unconstrained degree of freedom can move through the network by consecutive swapping operations. In Fig. 2.9b a degree of freedom is moved from the red node on the left to the green on the right by two consecutive swapping operations.
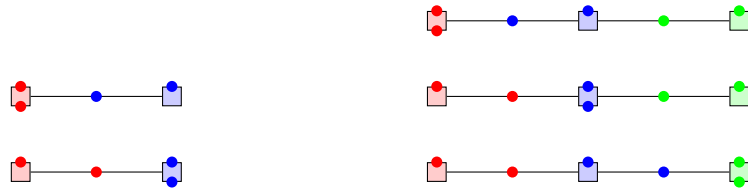
(a) Swapping an unconstrained degree of freedom from red to blue by replacing the pebble on the edge.

(b) By chaining swap operations the degree of freedom moves from red to blue to green.

Figure 2.9: Degrees of freedom can move around a network by swapping the pebble that covers an edge repeatedly.

The observation in the overconstrained square that it is impossible to end up with fewer than three unconstrained degrees of freedom is the basis for an algorithm that detects redundant edges. The algorithm iteratively adds one edge to the set of edges that have been visited. The edges in the visited set were either covered by a pebble or determined to be redundant. By repeatedly swapping pebbles on the visited part of the network it is always possible to assemble three pebbles (representing the rigid body motions) on the two nodes that the edge under consideration is incident to. If it is now possible to bring another, fourth, pebble to one of these nodes the considered edge will constrain it and it is covered by the pebble. If, however, it turns out there is not a free pebble, this edge edge cannot constrain any degree of freedom and is therefore marked as redundant and left uncovered. Fig. 2.10 shows this process from start to finish for the example overconstrained network of Fig. 2.8.

Searching the network for a pebble that can, through a series of swapping operations, be moved to once of the incident nodes can be implemented as traversing a directed graph. Only the edges that are covered by a pebble are part of this directed graph, not the edges that were deemed redundant, and neither the edges that have not been considered yet. Let the edges point from the node which covered that edge by one of its pebbles to the other. Now the search for a free pebble can be done by following the directed graph to all nodes that are reachable.

Now we can consider an example that has both a redundant edge and a floppy mode. We will apply the same procedure to the network in Fig. 2.11 as before, but we skip some intermediate steps that are analogous to the previous example. The final state in Fig. 2.11e can be interpreted to have all rigid body motions represented in the left triangle, while the right triangle can move independently from the rigid body motions because of the pebble on the green node. Similarly, it is possible to move two of the pebbles to the right part of the network, leaving the pebble on *e.g.* the red node (see Fig. 2.11f) that represents the floppy mode of the left part. Note, however, that it is impossible to move all four pebbles to one side.

Based on the observations we made in the previous part we can formulate a way of detecting rigid clusters within a network. When nodes are rigid with respect to each other they cannot contain more than the three rigid body motions' degrees of freedom. As soon as a fourth free pebble can be moved to the two nodes it is clear that the nodes are not rigid with respect to each other. After all edges have been either covered or deemed redundant another growth algorithm can be utilized to identify the rigid clusters. We will
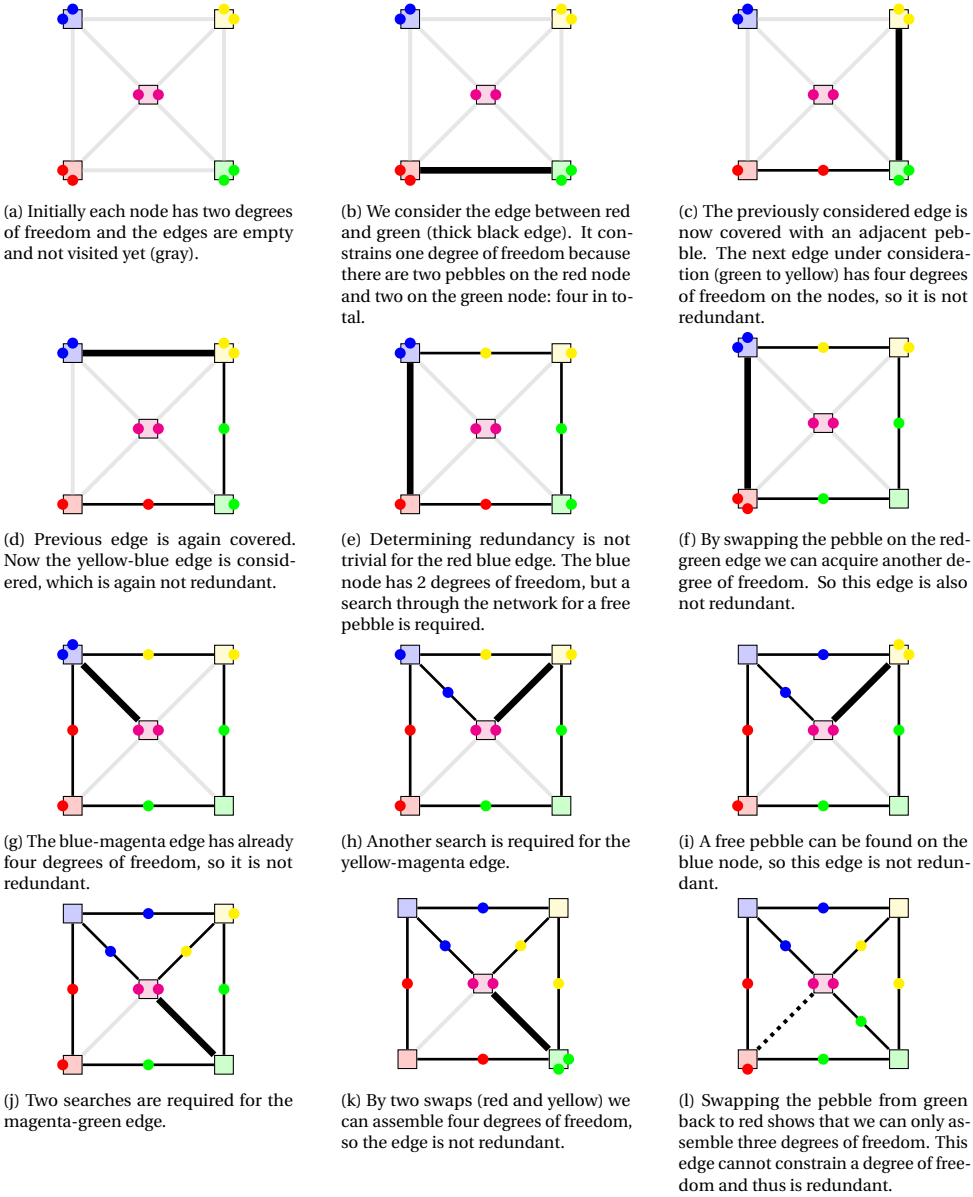
(a) Initially each node has two degrees of freedom and the edges are empty and not visited yet (gray).

(b) We consider the edge between red and green (thick black edge). It constrains one degree of freedom because there are two pebbles on the red node and two on the green node: four in total.

(c) The previously considered edge is now covered with an adjacent pebble. The next edge under consideration (green to yellow) has four degrees of freedom on the nodes, so it is not redundant.

(d) Previous edge is again covered. Now the yellow-blue edge is considered, which is again not redundant.

(e) Determining redundancy is not trivial for the red blue edge. The blue node has 2 degrees of freedom, but a search through the network for a free pebble is required.

(f) By swapping the pebble on the red-green edge we can acquire another degree of freedom. So this edge is also not redundant.

(g) The blue-magenta edge has already four degrees of freedom, so it is not redundant.

(h) Another search is required for the yellow-magenta edge.

(i) A free pebble can be found on the blue node, so this edge is not redundant.

(j) Two searches are required for the magenta-green edge.

(k) By two swaps (red and yellow) we can assemble four degrees of freedom, so the edge is not redundant.

(l) Swapping the pebble from green back to red shows that we can only assemble three degrees of freedom. This edge cannot constrain a degree of freedom and thus is redundant.

Figure 2.10: Complete process of determining redundant edges in the overconstrained square of Fig. 2.8

(a) Initial state of the network.

(b) The three edges in the yellow-magenta-green triangle are covered by pebbles by trivial searches.

(c) Two swaps are required to see that cyan-magenta is not redundant.

(d) Cyan-green is redudant as only three pebbles can be gathered.

(e) The triangle on the left is covered by trivial searches. Three rigid body motions are on the triangle on the left with a hinging mode represented by the pebble on the green node.

(f) At most two pebbles can be swapped to the right triangle, now representing the three rigid body motions there.
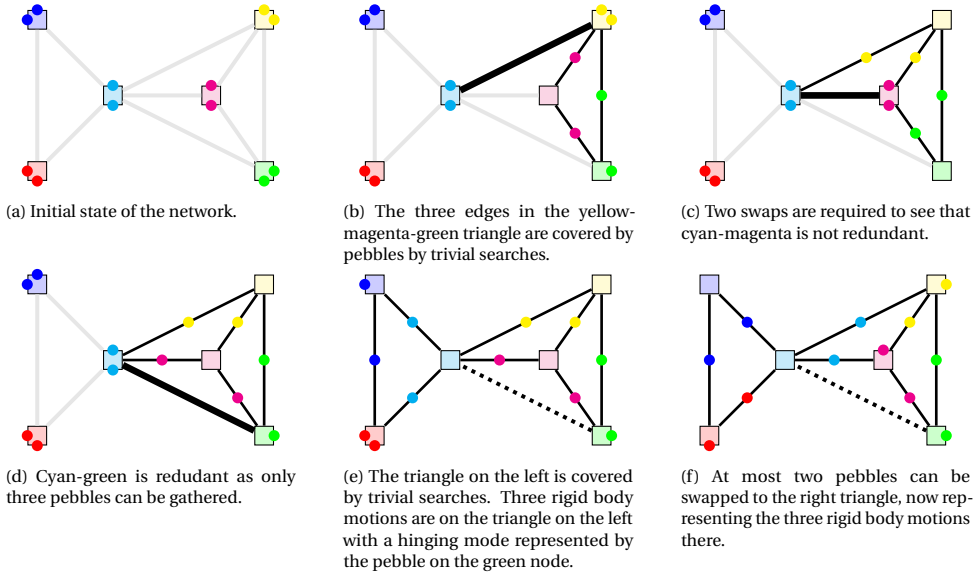
Figure 2.11: The pebble game applied to a simple network with a redundant edge and a floppy mode.

state the algorithm in general and apply it to the network in Fig. 2.11 as an example.

The algorithm starts by taking a random edge and collecting and pinning three pebbles on its two incident nodes. Now the set of edges that is rigid with respect to this starting edge is grown incrementally by the following procedure. Take an edge that is not yet part of any cluster and is incident to one of the nodes connected to the rigid cluster being grown. If it is impossible to move a pebble onto the node this edge is part of the cluster, otherwise it is not. This continues until there are no more unconsidered adjacent edges to the cluster; the cluster is now identified. If there are other unconsidered edges left in the network the growth of a new cluster starts by again picking a random unconsidered edge and growing a cluster from there.

Let us now, as an example, determine the rigid clusters in the same example as in Fig. 2.11, see Fig. 2.12. The first cluster is grown starting with the left most edge of the network, connecting the blue and red nodes. Only the next node in line is rigid with respect to these two: a pebble can be placed on the other nodes. The second cluster is grown starting from the edge between yellow and green. It grows to include the node in the middle, which acts as a hinge. All nodes around which clusters can hinge are part of at least two clusters.
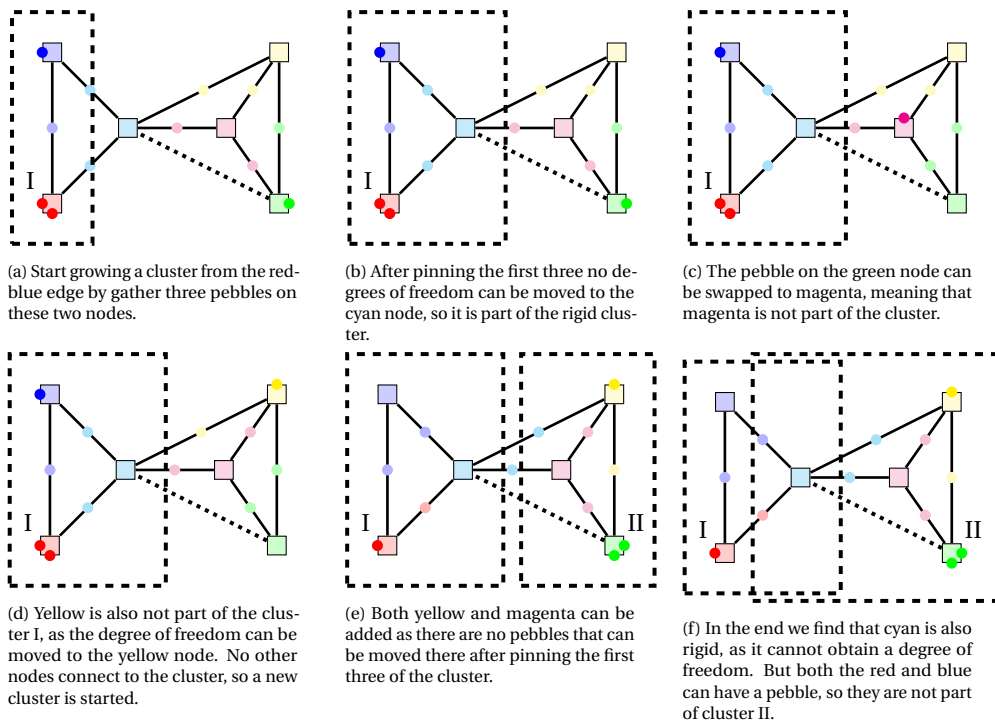
(a) Start growing a cluster from the red-blue edge by gather three pebbles on these two nodes.

(b) After pinning the first three no degrees of freedom can be moved to the cyan node, so it is part of the rigid cluster.

(c) The pebble on the green node can be swapped to magenta, meaning that magenta is not part of the cluster.

(d) Yellow is also not part of the cluster I, as the degree of freedom can be moved to the yellow node. No other nodes connect to the cluster, so a new cluster is started.

(e) Both yellow and magenta can be added as there are no pebbles that can be moved there after pinning the first three of the cluster.

(f) In the end we find that cyan is also rigid, as it cannot obtain a degree of freedom. But both the red and blue can have a pebble, so they are not part of cluster II.

Figure 2.12: Illustration of the process of determining rigid clusters in a network containing both a floppy mode and an over-constrained cluster.

2.6. APPENDIX: CATASTROPHIC CANCELLATION AT JAMMING

In simulations the real numbers describing quantities in physics such as positions are represented by a floating point number as specified in the IEEE standard ISO/IEC/IEEE 60559:2011. Floating point numbers have some notorious problems that require careful interpretation and evaluation of numerical results. Even something as innocuous as solving for the roots of a quadratic equation can be troublesome, see *e.g.* [59]. We will show two problems that arise when preparing packings close to the jamming transition: catastrophic cancellation in the overlap and a non-uniform resolution. For the sake of illustration we will represent floating point numbers as decimal numbers with five digits in the significand or mantissa and two digits in the exponent, for example $1.2345 \cdot 10^{-02}$.

In every subtraction of two floating point numbers that share the first few digits a rounding error is introduced. This error grows as the numbers become more similar. An example of a large rounding error is

$$
\begin{array}{r}
1.2345 \cdot 10^{-02} \\
1.2334 \cdot 10^{-02} \\
\hline
1.1xxx \cdot 10^{-05}
\end{array}
\tag{2.4}
$$

where x denotes a digit that cannot be computed with rounding error. The rounding error can get arbitrarily large as the numbers get closer together.

In the expression of the overlap we find exactly such a subtraction when trying to go to the limit of zero pressure. In this limit the particles are barely touching which results in the dimensionfull overlap r_{ij} going towards $\sigma_i + \sigma_j$.

When approaching the transition closely or when applying very small deformations to the box shape this results in unexpected jumps in the energy and gradient. The main conclusion of this analysis is that the precision of the underlying floating point number sets a threshold to how close the transition can be approached. Conversely this means that we can get closer to the transition by increasing the precision of the numbers that represent positions. Most machines do not go beyond 64 or 80 bits per number, however there are two standard techniques to create higher precision numbers from other data structures. A relatively slow, but arbitrary precision solution is storing numbers as an arbitrarily long sequence of characters or words, see *e.g.* [60–62]. We see a composition of two or more standard floating point numbers as a more viable solution to increase precision enough for the simulation requirements, see *e.g.* [63–65]. The basic idea is to keep the significand of the two numbers exactly contiguous during all arithmetic operations. In the implementation developed in this thesis it is possible to use two of the largest number types available: 128 or 160 bits depending on compiler and CPU architecture.

Furthermore the same problem arises when considering perturbations to the energy. A small deformation of the box will to leading order result in a second order perturbation of the energy in the strain. Subtracting the constant energy of the initial state from the measured energy can be so close for small strains that again catastrophic cancellation occurs. The limit of small strains is of interest when comparing an actual deformation with a linearization of the packing, as the likelihood of a contact change over the strain

interval decreases. Note that the gradient does not exhibit this, as it is always expanded around zero, *i.e.* a state of mechanical equilibrium.

2

3

ELASTICITY IN ATTRACTIVE SOFT DISK PACKINGS

Numerous soft materials jam into an amorphous solid at high packing fraction. This non-equilibrium phase transition is best understood in a model system where particles repel when they overlap. Recently, however, it was shown that introducing any finite amount of attraction between particles changes the universality class of the transition. The properties of this new "sticky jamming" class remain almost entirely unexplored. We use molecular dynamics simulations and scaling analysis to determine the shear modulus, bulk modulus, and coordination of marginal solids close to the sticky jamming point. Each observable differs not just quantitatively but also qualitatively from the purely repulsive case.
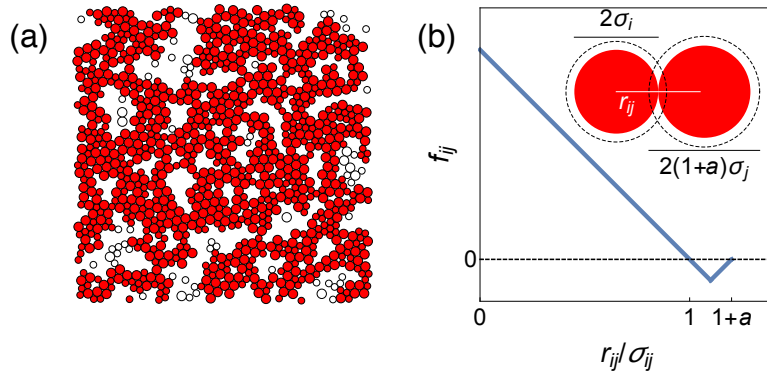
Figure 3.1: (left) A periodic packing of sticky disks at $\phi \approx \phi_c$. Red disks participate in the spanning rigid cluster. (right) Their force law. The dimensionless parameter a sets the range and strength of the attractive interaction; $a = 0.1$ at left.

Non-Brownian dispersions, including emulsions, foams, and pastes, jam into amorphous solids above a critical packing fraction [66]. Nearly all numerical and theoretical studies of the jamming transition employ a (by now canonical) model where athermal spheres repel when they overlap [1, 2, 14]. Nevertheless, soft matter generically displays some degree of "stickiness," e.g. due to depletion interactions in emulsions [25, 26, 67], finite contact angles in foams [68], or liquid bridges in wet granular media [12, 27, 28, 51] and capillary suspensions [69].

We expect the jamming scenario for sticky particles to be relevant to a broad range of natural and engineered systems where attraction is generically present. Nevertheless, many of the fundamental mechanical and structural properties of sticky jammed matter remain unexplored. The relatively few studies of sticky soft spheres that are available reveal important differences from repulsive jamming: (i) sticky particles jam at lower packing fractions, with structural signatures reminiscent of gels [33, 34]; (ii) they form shear bands under conditions where repulsive particles do not [35–37, 70]; and (iii) most tellingly, they belong to a distinct universality class [39]. In fact, any finite attraction between particles places a system in the sticky jamming class [71].

What distinguishes sticky jammed solids from their repulsive counterparts? In repulsive jamming, the elastic moduli and mean coordination display power law scaling as a function of distance to the critical packing fraction [1, 2]. While it seems plausible that similar scaling relations exist near sticky jamming, this hypothesis has not been tested. Here we study critical scaling in marginally jammed packings of sticky disks (Fig. 1a) and show that they depart qualitatively from the repulsive jamming scenario in three distinct ways. First, the shear modulus G vanishes with a critical exponent that is much larger than its repulsive counterpart. Second, the bulk modulus K also vanishes continuously at the sticky jamming point, unlike the discontinuous transition seen in repulsive systems. Finally, constraints on motion (i.e. bonds) outnumber particulate degrees of freedom at the sticky jamming transition. Balance between the two, or isostaticity, is specific to repulsive jamming.

3.1. MODEL

We consider the same model treated in Chapter 2. For clarity we re-iterate the main features here.

We consider systems of $N = 1024$ particles in $d = 2$ dimensions prepared in a periodic square cell. Each particle has a disk-shaped core of radius σ_i and an annular shell of thickness $a\sigma_i$. We use the standard 50:50 bidisperse mixture with a size ratio of 1.4:1 [1, 42], and take the core diameter of the small disks as our unit of length. The finite-ranged force between disks is a piecewise function of the overlap $\delta_{ij} = \sigma_{ij} - r_{ij}$, where $\sigma_{ij} = \sigma_i + \sigma_j$ and r_{ij} is the distance between their centers,

$$f_{ij} = \begin{cases} k\delta_{ij} & \delta_{ij} \geq -a\sigma_{ij} \\ -k(\delta_{ij} + 2a\sigma_{ij}) & -a\sigma_{ij} > \delta_{ij} \geq -2a\sigma_{ij} \\ 0 & \delta_{ij} < -2a\sigma_{ij}. \end{cases} \tag{3.1}$$

See also Fig. 1b. This force law is chosen both for its simplicity and for consistency with prior work [33–37, 39, 71]. Overlapping cores contribute a repulsive spring-like interaction with stiffness $k = 1$, which fixes our units of stress. Overlap between outer shells gives an attractive contribution; the parameter a fixes both its range and the maximum tensile force. We use this dimensionless number to characterize attraction strength.

For each attraction strength and packing fraction ϕ, calculated from the cores, systems are prepared by randomly placing particles in the unit cell and quenching to a local energy minimum using a nonlinear conjugate gradient algorithm [42]. Each system is analyzed with the standard pebble game algorithm [3], which yields a complete set of rigid clusters and redundancies. A rigid cluster is a set of connected particles with no zero frequency eigenmodes, apart from trivial rigid body motions. A redundancy is a set of bonds, any one of which can be removed from their cluster without loss of rigidity. For each redundancy there is a corresponding state of self-stress (SSS), a balanced configuration of forces compatible with the system's contact network. While redundancies arise naturally in the context of the pebble game, SSS's are more widely discussed in the literature – see e.g. [5, 9, 72–75]. We refer to a system as rigid/jammed if it contains a rigid cluster that spans the unit cell. For each jammed state the shear modulus G and bulk modulus K are calculated in the harmonic approximation by inverting the Hessian matrix, as detailed in Refs. [6, 76]. Data for each (a, ϕ) pair are averaged over 100-1000 samples. Standard errors are smaller than the plotted symbols.

Repulsive systems jam at $\phi = \phi_c(0) \approx 0.84177$ [77]. In attractive systems a spanning cluster appears instead at $\phi_c(a) = \phi_c(0) - \epsilon(a)$, where $\epsilon(a)$ represents the volumetric strain needed to compress the system from $\phi_c(0)$ to $\phi_c(a)$. In the previous Chapter we found that

$$\epsilon(a) \simeq \left(\frac{a}{a_0} \right)^\nu, \tag{3.2}$$

with $\nu = 0.5$ and $a_0 = 0.80$ [71]; here we take these values as given. In the same study, we showed that cluster size statistics display finite size effects when $a < a^* \sim 1/N$. We focus here on $10^{-3} \leq a \leq 10^{-1}$.

3.2. SHEAR MODULUS

We first consider the shear modulus G as a function of packing fraction and attraction strength. In Fig. 3.2a one sees that, for each value of a, G vanishes continuously at a ϕ that corresponds closely to $\phi_c(a)$ determined from rigid cluster percolation (colored arrows). For the smallest attraction strengths in Fig. 1a (where $a \simeq a^*$), the modulus resembles its form in repulsive jamming, $G_0(\phi)\,\Theta(\Delta\phi_0)$, where $\Theta(x)$ is the unit step function and $G_0 \equiv g_0\,\Delta\phi_0^\mu$ with $g_0 \approx 0.22$, $\Delta\phi_0 \equiv \phi - \phi_c(0)$, and $\mu = 1/2$ [1]. The initial growth of G becomes shallower with increasing a, and any resemblance to the repulsive shear modulus is lost.

We now show that $G(\phi, a)$ can be expressed in terms of a master curve that depends on a single variable α. We first define $\mathscr{G}_\pm$ as the ratio between the sticky and repulsive shear moduli at the same value of $|\Delta\phi_0|$, $\mathscr{G}_\pm \equiv G(\phi, a)/|G_0|$. The function has two branches, one for each sign of $\Delta\phi_0$. We then motivate α in the following way. Near the sticky jamming point, we expect that G will grow as a power law $G \sim f(a)\,[\phi - \phi_c(a)]^\psi$. (The prefactor $f(a)$ will be discussed below.) Deep in the sticky jammed phase, tensile forces are rare and packings resemble purely repulsive systems. We therefore anticipate that $G \simeq G_0 \sim \Delta\phi_0^\mu$ will be recovered. The crossover between these two scaling relations must be governed by the distances $\phi - \phi_c(a) = \Delta\phi_0 + \epsilon(a)$ and $|\Delta\phi_0|$. Their ratio is a function of

$$\alpha \equiv \left(\frac{\epsilon}{|\Delta\phi_0|}\right)^{1/\nu} \simeq \frac{a/a_0}{|\Delta\phi_0|^{1/\nu}} \,. \tag{3.3}$$

For later convenience we have defined α so as to be linear in a. By construction the jamming point is at $\alpha_c = 1$ and jammed states have $\alpha \geq 1$. Finally, we make the scaling ansatz that $\mathscr{G}_\pm$ is a function of α,

$$\frac{G(\phi, a)}{|G_0|} = \mathscr{G}_\pm(\alpha)\,. \tag{3.4}$$

We emphasize that Eq. (3.4) depends only on known quantitites: the repulsive jamming point $\phi_c(0)$ [77]; the repulsive shear modulus (exponent $\mu = 0.5$) [1]; and the shift in the sticky jamming point ϵ determined from rigid cluster analysis (exponent $\nu = 0.5$) [71]. Eq. (3.4) is therefore a prediction without any free parameters.

Fig. 2b verifies the data collapse predicted in Eq. (3.4). The upper branch $\mathscr{G}_+$ approaches unity when α vanishes, i.e. the modulus for repulsive jamming is recovered. The lower branch $\mathscr{G}_-$ vanishes for states below $\alpha \approx 1$, indicative of unjamming. (The same data are plotted versus $\alpha - 1$ in the inset.) Some states do exist slightly below $\alpha = 1$; we attribute this to finite size effects, which smear out $\phi_c(a)$ [71]. It is apparent that there is also a third scaling regime, in which both branches scale as $\mathscr{G}_\pm \sim \alpha^\Delta$ for some positive exponent Δ. This expression describes the shear modulus when $\phi \approx \phi_c(0)$. Since G remains finite at $\phi_c(0)$ when a is nonzero, any dependence on $\Delta\phi_0$ must be subdominant. This requirement is only satisfied if $\Delta = \mu\nu = 0.25$.

We now apply data fitting to the master curve in Fig. 3.2b to estimate the exponent ψ that describes the initial growth of G above the sticky jamming point. As stated above, we anticipate

$$G \simeq f(a)\,[\phi - \phi_c(a)]^\psi, \tag{3.5}$$

for some $\psi > 0$. The prefactor $f(a)$ is present because there is no reason to forbid it. We now assume $f \simeq c_G\,a^{-\omega}$ to leading order. Importantly, the exponent ω is not free; it is only
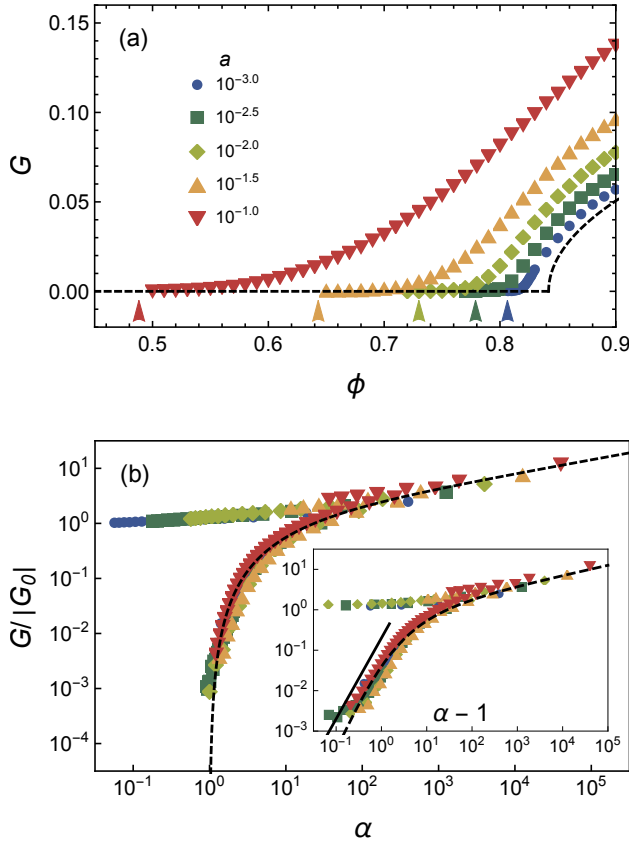
Figure 3.2: (a) The shear modulus of sticky packings at varying attraction strength a. The legend applies to this and all subsequent figures in the Chapter. The dashed curve is G for $a = 0$. Arrows indicate $\phi_c(a)$ according to Eq. (3.2). (b) Data collapse of the shear modulus according to Eq. (3.4). (inset) The same data plotted versus $\alpha - 1$. The dashed curves depict Eq. (3.6) with $\psi = 2.5$. The solid line has slope 2.

compatible with Eq. (3.4) if $\omega = \nu\psi - \Delta$. Hence if the shear modulus obeys Eq. (3.5) near $\phi_c(a)$, the lower branch of the scaling function must scale as

$$\mathscr{G}_- \simeq c_G \, \alpha^\Delta \left[1 - \alpha^{-\nu}\right]^\psi \tag{3.6}$$

sufficiently close to $\alpha = 1$. Eq. (3.6) has a crossover from $\mathscr{G}_- \sim (\alpha - 1)^\psi$ as $\alpha \to 1^+$ to $\mathscr{G}_- \sim \alpha^\Delta$ when $\alpha \to \infty$. Therefore we can estimate ψ in two ways: first, by fitting $(\alpha - 1)^\psi$ to data at small $\alpha - 1$; or, second, by fitting a wider range of data with Eq. (3.6). The first approach is rigorous and preferable when many decades of data in $\alpha - 1$ are available below the crossover. As our data covers less than two decades, fitting to $(\alpha - 1)^\psi$ can erroneously lower the estimate of ψ. The second approach "knows about" the crossover and so allows one to fit to more data. But it is also less rigorous, because it is not *a priori* clear how far from $\alpha = 1$ the Eq. (3.6) holds. Recall that $\mathscr{G}_- \sim \alpha^\Delta$ as $\alpha \to \infty$ is required as a consequence of the scaling collapse in Fig. 3.2b. As Eq. (3.6) matches this form, we
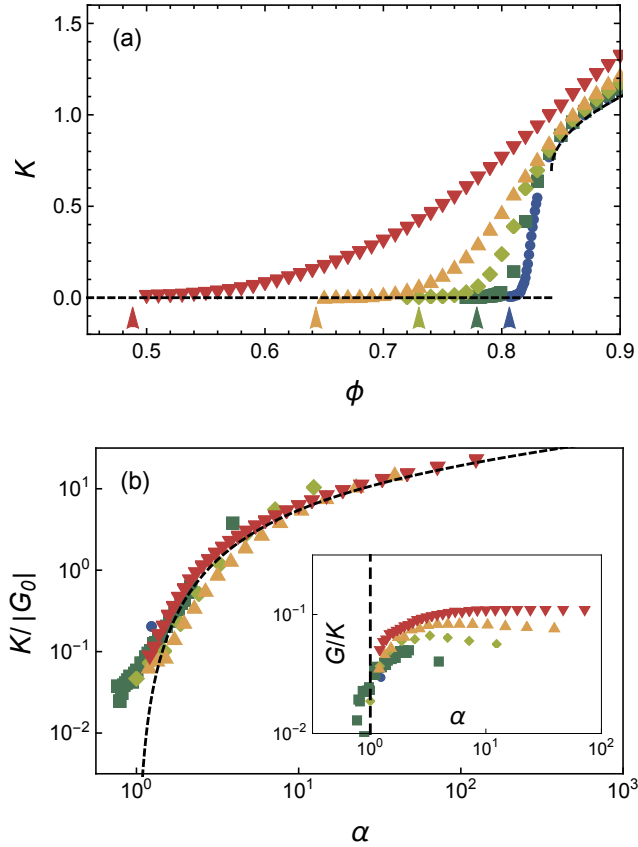
3

Figure 3.3: (a) The bulk modulus of sticky disk packings at varying attraction strength a. The dashed curve shows K for $a = 0$. (b) The rescaled bulk modulus for $\phi \leq 0.81$ plotted versus α. The dashed curve depicts $11.1\, c_G\, \alpha^\Delta\, [1 - \alpha^{-\nu}]^\psi$ with $c_G = 0.81$ and $\psi = 2.5$, as in Fig. 3.2b. (inset) The ratio of shear to bulk modulus, also for $\phi \leq 0.81$.

attempt to fit it to the entire lower branch. One could write down other functions that cross over between the same power law scalings as Eq. (3.6), and this choice may influence the fitted value of ψ. The result of the first approach is depicted by the solid curve in Fig. 3.2b. We find $\psi = 2.0$ (hence $\omega = 0.75$). Fitting the lower branch to Eq. (3.6) yields instead $\psi = 2.5$ ($\omega = 1.0$), with $c_G = 0.81$ – see the dashed curve. We therefore expect that the critical exponent is at least 2.0 and likely in the interval $\psi \in [2.0, 2.5]$. We emphasize that ψ is clearly larger than the corresponding exponent μ in repulsive packings, which signals the distinct mechanical character of sticky jammed matter.

3.3. BULK MODULUS

Next we consider the bulk modulus K as a function of packing fraction while varying attraction strength, as shown in Fig. 3.3a. The sticky modulus is always continuous, with

a steep slope near $\phi_c(0)$ for the smallest values of a. For context, we recall that for purely repulsive particles with harmonic interactions, the repulsive bulk modulus vanishes discontinuously at $\phi_c(0)$ (Fig. 3.3a, dashed curve), unlike the repulsive shear modulus. The jump has been shown to result from self-organization into a state that can support isotropic stress without tensile forces [17, 78]. Closely related systems such as randomly pruned spring networks, which do not self-organize and do permit tensile forces, have a continuous K that vanishes with the same exponent as G [79]. Tensile forces are also present in sticky packings, which suggests the latter scenario may be relevant near $\phi_c(a)$.

It is therefore reasonable to ask if the bulk modulus and the shear modulus have the same scaling near the sticky jamming point, i.e. if $K \sim a^{-\omega} [\phi - \phi_c(a)]^{\psi}$ with the same exponent ψ (and hence ω as well). As a first check, we focus on packing fractions $\phi \leq 0.81$, well below $\phi_c(0)$, and rescale K in the same way we rescaled G in Fig. 3.2b; namely, we plot $K/|G_0|$ versus α. (Note that it is not essential to divide by $|G_0|$, any multiple of $|\Delta\phi_0|^{\mu}$ would work.) We then look to see if, as in Eq. (3.6), the rescaled data scale as $\alpha^{\Delta} [1 - \alpha^{-\nu}]^{\psi}$ for some range of α. This test is shown in Fig. 3.3b. While there is more scatter than in Fig. 3.2b, the data are indeed reasonably described by the same scaling relation as G using $\psi = 2.5$. This result should be interpreted cautiously, however, as a plot of the ratio G/K (Fig. 3.3b, inset) reveals additional subtlety. If G and K vanish with the same exponent, each curve should approach a finite value as $\alpha \to 1^{+}$. Instead the data turn downwards in the vicinity of $\alpha = 1$. This could be due to a bulk modulus exponent ψ' that is slightly smaller than the shear exponent ψ. Alternatively, it may be a finite size effect.

3.4. Coordination and redundancies

The coordination of a network characterizes its structure and plays a fundamental role in theories of the moduli in repulsive jamming, e.g. [17, 80]. It is therefore useful to identify correlations between coordination and packing fraction.

Let us first recall the main result of Maxwell-Calladine counting, which relates degrees of freedom, constraints on motion, floppy modes, and redundancies in a network of nodes and bonds (viz. particles and contacts) [9]. It states that $d - \frac{1}{2}z = n_f - n_r + O(1/N)$, where z is the coordination averaged over nodes, and n_f and n_r are the numbers of floppy modes and redundancies per node, respectively. Neglecting the $O(1/N)$ correction and applying this relation to a spanning rigid cluster, which has no floppy modes, gives $z = z_{\text{iso}} + 2n_r$, where $z_{\text{iso}} \equiv 2d$ is the Maxwell isostatic value. Therefore creating new contacts, e.g. by compression, also introduces an equal number of redundancies. While Maxwell-Calladine counting places no further constraints on n_r, it is an empirical fact that n_r vanishes at the jamming point in repulsive systems [1, 81–83], i.e. $z_c(a = 0) = z_{\text{iso}}$. In fact, $z = z_{\text{iso}}$ is often used as a criterion for jamming. Given this context, in Fig. 3.4a we plot n_r versus ϕ for varying a. Unlike repulsive systems, n_r remains finite as ϕ approaches $\phi_c(a)$, indicating that the spanning cluster is overconstrained, $z_c(a) > z_{\text{iso}}$. Hence Maxwell's isostatic value does not signal rigidity percolation in sticky systems.

In order to quantify the critical redundancy density $n_c(a) \equiv n_r(\phi_c(a))$, we investigate the point where the shear modulus vanishes in a plot of G versus n_r, as shown in the inset of Fig. 3.4b. We have verified that the bulk modulus also vanishes at the same redundancy density (not shown). We seek to collapse the data by plotting $G/(a/a_0)^{\delta}$ versus $n_r/(a/a_0)^{\delta}$. The same exponent δ must appear on each axis to ensure that the
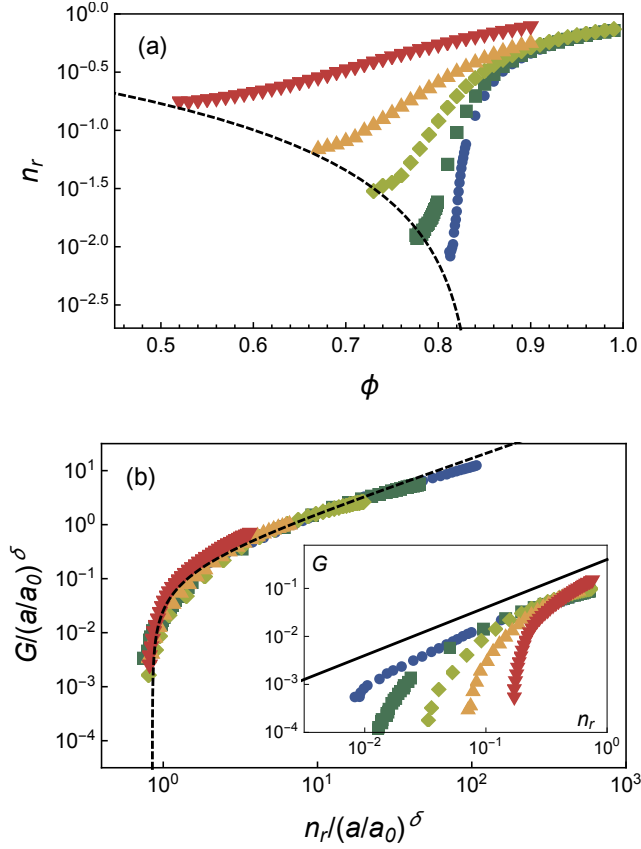
Figure 3.4: (a) The redundancy density n_r plotted as a function of packing fraction for varying attraction strength. The dashed curve shows $n_c \sim [\phi_c(0) - \phi_c(a)]^{\delta/\nu}$. (b) Collapse of the shear modulus with n_r when both are rescaled with a^δ. $G \sim n_r - n_c$ (dashed curve) is plotted for comparison. (inset) Unscaled data. The solid line has slope 1.

known form for repulsive systems, $G \sim n_r$ [1, 17], is recovered when $a \to 0$. We find good data collapse for $\delta = 0.75$, with the master curve vanishing at a value $n_0 \approx 0.85$ on the abscissa (Fig. 3.4b, main panel). It follows that $n_c \simeq n_0 \, (a/a_0)^\delta$, and that the excess coordination at the sticky jamming point is $z_c(a) - z_{iso} = 2n_c \sim [\phi_c(0) - \phi_c(a)]^{\delta/\nu}$ (Fig. 3.4a, dashed curve). Above the sticky jamming point, the expression $G \sim n_r - n_c$ represents a natural generalization of the repulsive case and provides a reasonable fit to our data (dashed curve, Fig. 3.4b main panel). In other words, G grows in proportion to the number of excess redundancies compared to the spanning cluster at percolation.

3.5. DISCUSSION

We have shown that sticky jamming differs from repulsive jamming in three distinct ways. While the shear modulus in repulsive packings vanishes continuously with a critical exponent $\mu = 1/2$, in sticky jamming the exponent $2.0 \lesssim \psi \lesssim 2.5$ is much larger. The

bulk modulus in sticky systems vanishes continuously and apparently in proportion to G, unlike repulsive jamming where it has a jump. And redundancies persist at the sticky jamming point, with number density $n_c \sim a^{\delta}$ and $\delta \approx 0.75$. In contrast, $n_c = 0$ at repulsive jamming.

The mechanical and structural properties identified here represent a challenge to existing theories of elasticity in marginal solids [17, 78, 80, 84]. A successful theory should predict the values of the exponents ψ, δ, and ν, each of which remain empirical. Effective medium theories for marginal elastic solids predict both G and K to vanish continuously [84]; however, they do not successfully account for the repulsive case [79]. While there is a successful theory of elasticity in repulsive jammed solids [17], a straightforward generalization of its results would predict both G and K are *dis*continuous at sticky unjamming due to the presence of redundancies. More qualitatively, we are not aware of any theory that predicts unjamming with $n_c > 0$, and hence $z > z_{\mathrm{iso}}$.

We see several directions for future work. Most obviously, the measurement of the shear exponent ψ should be improved. Similarly, one should determine more conclusively whether the same exponent describes the bulk modulus. Both tasks can be achieved with a data set that accesses smaller values of $\alpha - 1$ and larger system sizes. This will also permit an analysis of finite size effects and corrections to scaling. Next, simulations in three dimensions are needed. While we expect critical scaling to persist, the exponents ψ, δ, and ν may differ, as is the case for other exponents near sticky jamming [39]. In addition, the force law in Eq. (3.1) is particularly simple, with just one parameter a; untangling the role of, e.g., the maximum tensile force and the range of the interaction will facilitate comparisons to experiment. Finally, it is natural to ask how sticky systems respond to oscillatory shear, which would build a bridge between the present work, viscoelasticity in repulsive jamming [6, 23, 47, 85], and steady shear flow in sticky systems [36, 37].

3

4

THE JAMMING POINT IN BIDISPERSE DISK PACKINGS

We systematically map out the jamming transition of all 2D bidisperse mixtures of frictionless disks in the hard particle limit. The critical volume fraction, mean coordination number, number of rattlers, structural order parameters, and bulk modulus each show a rich variation with mixture composition and particle size ratio, and can therefore be tuned by choosing certain mixtures. We identify two local minima in the critical volume fraction, both of which have low structural order; one minimum is close to the widely studied 50:50 mixture of particles with a ratio of radii of 1:1.4. We also identify a region at low size ratios characterized by increased structural order and high rattler fractions, with a corresponding enhancement in the stiffness.
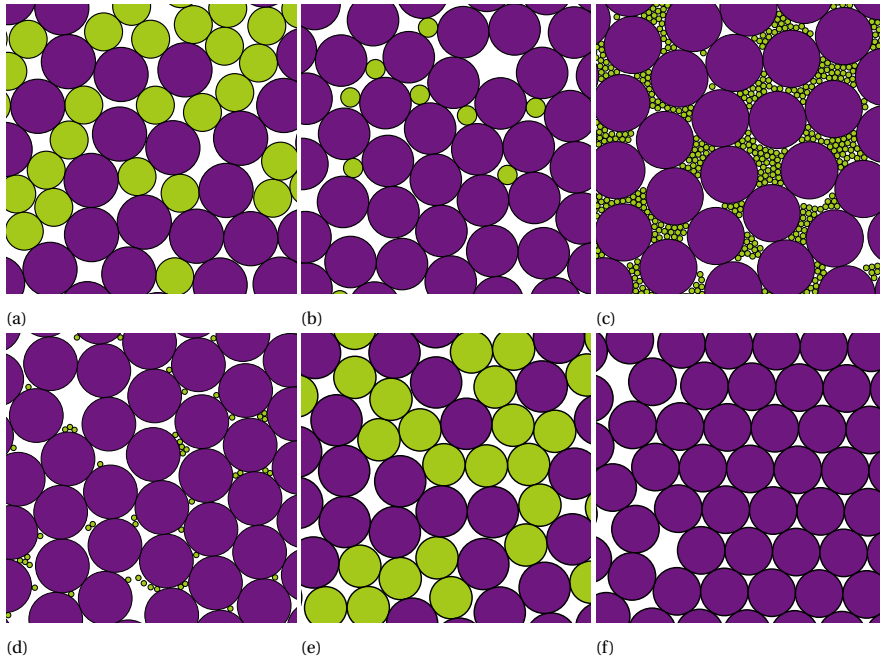
Figure 4.1: Bidisperse disk packings taken from the correspondingly labeled points in fig. 4.3b.

Soft materials such as foams, emulsions, and granulates exhibit a nonequilibrium fluid-solid, or "jamming", transition when their density is increased. While most jammed matter is three-dimensional, jammed structures also occur in 2D when particles are trapped at interfaces, *e.g.* in bubble rafts, Pickering emulsions and ice flows. Numerous scaling exponents characterizing geometry and mechanics are also found to be the same in 2D and 3D [2, 83]. As simulations in 2D are also (comparatively) computationally inexpensive, studies of jammed disk packings feature prominently in the literature [1, 2, 22, 77, 83, 86–90].

Disorder is a distinguishing feature of jammed packings [91–95], and indeed the critical volume fraction ϕ_c where frictionless packings jam is often denoted random close packing (RCP), although this name is controversial [96]. Unlike spheres, rapidly quenched monodisperse disk packings tend to crystallize – hence bidisperse mixtures are widely favored (fig. 4.1). By convention, most studies consider the 'classic' mixture of small and large disks – a 50:50 ratio of the number of disks with a 1:1.4 size ratio of their radii [1, 97, 98] – selected for their low degree of structural order, see *e.g.* [1, 2, 22, 77, 83, 86–88, 97, 98]. Far less is known about other number and size ratios [89, 90, 99–105]. The goal of the present work is to systematically map the space of bidisperse frictionless disk mixtures for the first time.

We have several main findings. By varying the number ratio f_n and size ratio f_r, we find rich structure in $\phi_c(f_r, f_n)$, including a large region with low ϕ_c and low structural order appropriate to studies of jamming. This region includes the 'classic' mixture, which

is close to the global minimum of ϕ_c. However there is a second local minimum which, to our knowledge, has not previously been reported; this minimum may be of particular interest for future jamming studies. We find that ϕ_c increases dramatically for mixtures with extreme difference in their radii, as small particles fill in the voids formed by large particles. These and other mixtures exhibit local crystalline order and a high number of non-load bearing particles (rattlers), which both correlate strongly and positively with the bulk modulus. Hence it may be possible to use mixture composition and size ratio to tune stiffness.

4.1. MODEL AND METHODS

Bidisperse mixtures contain N_a particles with radius R_a and N_b particles with radius R_b. Packings are characterized by the number fraction $f_n = N_a/(N_a + N_b)$ and size ratio $f_r = R_a/R_b$. The space of all bidisperse mixtures is then given by $0 \le f_n \le 1$ and $0 \le f_r \le \infty$. On five lines in this domain the mixture is monodisperse: $f_r = 0$, $f_r = 1$, $f_r = \infty$, $f_n = 0$ and $f_n = 1$. Furthermore, any point (f_r, f_n) in the domain represents the same mixture as the point $(1/f_r, 1 - f_n)$, except for a change of scale. We therefore consider only mixtures where $f_r \le 1$. The remaining (f_r, f_n) parameter space is sampled with a regular 41×41 grid.

Our simulations approach ϕ_c from the jammed phase, using soft particles with a finite ranged repulsive potential

$$U_{ij} = \begin{cases} (k/2)\left(R_i + R_j - r_{ij}\right)^2 & R_i + R_j \ge r_{ij} \\ 0 & R_i + R_j < r_{ij}. \end{cases} \tag{4.1}$$

Here k is the spring constant and sets the energy scale, r_{ij} is the center-to-center distance between particles i and j, and R_i is the radius of particle i. The unit of length is set by the radius of the larger particle, $R_b = 1$.

We use 2D packings of $N = N_a + N_b = 1024$ particles (unless stated otherwise) generated by instantaneously quenching an infinite temperature configuration to a local energy minimum using the nonlinear conjugate gradient method of [77]. Packings are created at a specified ϕ, yielding an ensemble with a distribution of pressures [86]. The criterion for jamming is the same as in [77], *viz.* the energy is larger than a low threshold. Fig. 4.2 shows the fraction of jammed packings f_j versus ϕ. The location of the jamming transition for a certain f_r and f_n is taken as the value ϕ_c where half of the packings are jammed, *i.e.* $f_j(\phi_c) = 0.5$. We estimate ϕ_c from a regression through five points close to $f_j = 0.5$, see fig. 4.2 (inset). At every ϕ there is a statistical uncertainty associated with the binomial distribution of finding a jammed packing. The resulting uncertainty is at most 0.006 in ϕ_c, estimated with the largest deviation from the regression line.

4.2. JAMMING OF MIXTURES

We find rich structure in the location of the jamming transition $\phi_c(f_r, f_n)$, as depicted in both surface and contour plots in fig. 4.3. Several features stand out: flat lines along the domain edges; a clear peak in ϕ_c in the upper corner, with a corresponding ridge; and two basins around local minima, labeled **b** and **e**. We discuss each feature in turn.
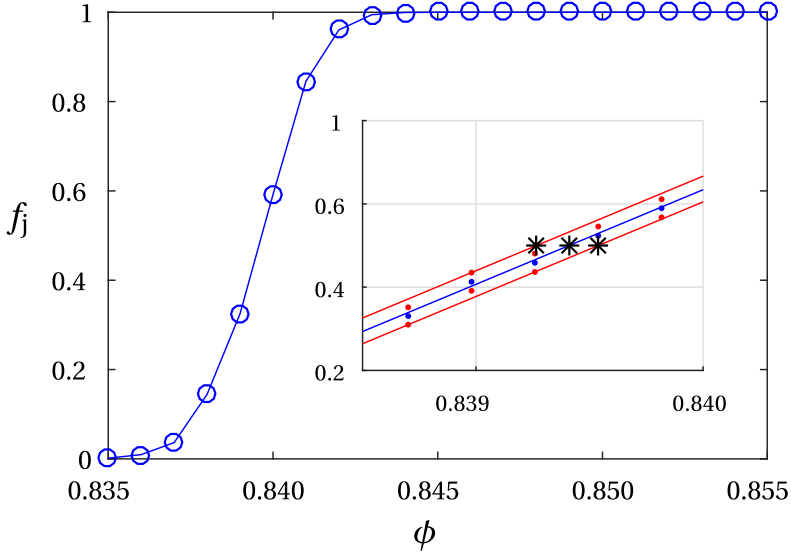
Figure 4.2: Fraction of jammed packings f_j at different packing fractions ϕ, for $f_r = 0.7$ and $f_n = 0.5$. (inset) ϕ_c is estimated with linear regression on five points in the linear part of this curve. The stars indicate the estimate for ϕ_c and the error bounds.

Flat edges.– The edges of the domain correspond to monodisperse mixtures. Hence ϕ_c is constant, though not that of a triangular lattice due to defects, the cause of which we discuss in more detail later. Along the edge $f_r = 0$ we find stronger finite size effects, since $R_a = 0$ and so the effective number of particles changes with f_n. Near this edge minimizing the energy is numerically challenging due to strong separation of scales in the two radii. In this region there is a slight systematic overestimate of the jammed fraction f_j for packings close to jamming, resulting in a small underestimate of ϕ_c.

The critical volume fraction falls off sharply upon moving away from three of the four domain edges, which suggests even weak bidispersity inhibits structural order. We find radically different behavior moving away from the edge $f_r = 0$. Here ϕ_c first increases, hinting that packings at low f_r are qualitatively different in their structure.

Ridge and peak.– When $f_r < f_r^* = 2/\sqrt{3} - 1$ (dotted line in fig. 4.3b) the small species fits within the void formed by a triangle of large particles (visible in figs. 4.1c,4.1d). In this region many of the small particles are 'rattlers' (they bear no load), hence are effectively not part of the contact network, as can be seen from the linear increase of small rattler fraction ρ_s in fig. 4.4a. Due to void filling, high critical packing fractions are reached along this edge, exceeding even $\phi_{xtal} \approx 0.9069$ of the monodisperse triangular lattice. When following a line of fixed f_r from small to large f_n (corresponding to the ridge in ϕ_c), we depart from a monodisperse packing of large particles by introducing rattlers in the (mostly triangular) voids formed by large particles. Filling continues until for some f_n there are enough small particles that they frustrate the jammed structure of large particles and simultaneously become load-bearing particles – see the sharp decrease in ρ_s in fig. 4.4a.

(a)

(b)
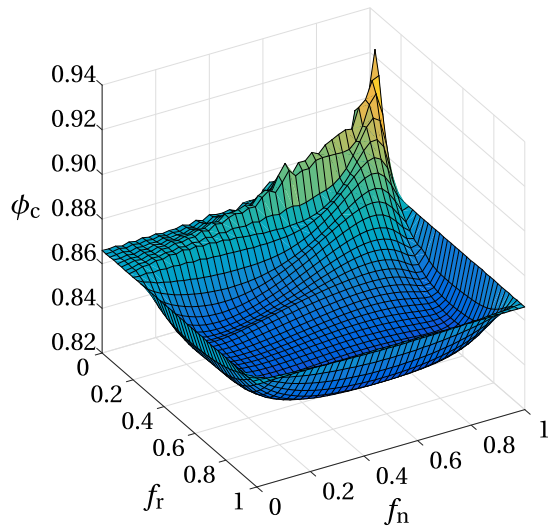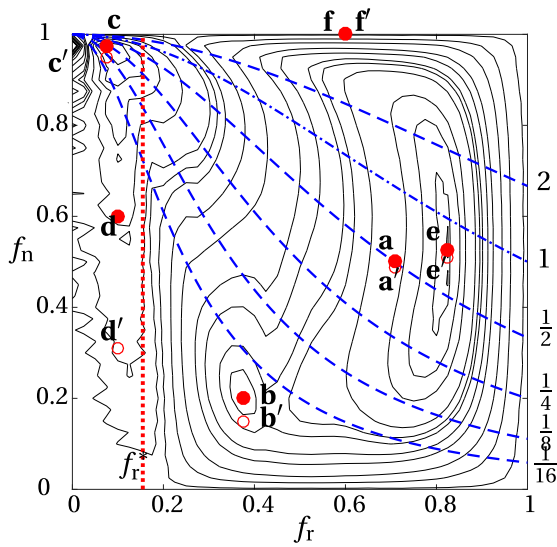
Figure 4.3: (a) ϕ_c surface as a function of number and size ratio. (b) Contours of the same surface. The (dot-)dashed curves follow constant ratio of species volume (value indicated on the right). Voids in a triangle of large particles can hold at least one small rattler for $f_r < f_r^*$. Mixtures that are discussed are marked (see fig. 4.1); a prime denotes the shift of the point when using the corrected f_n'.
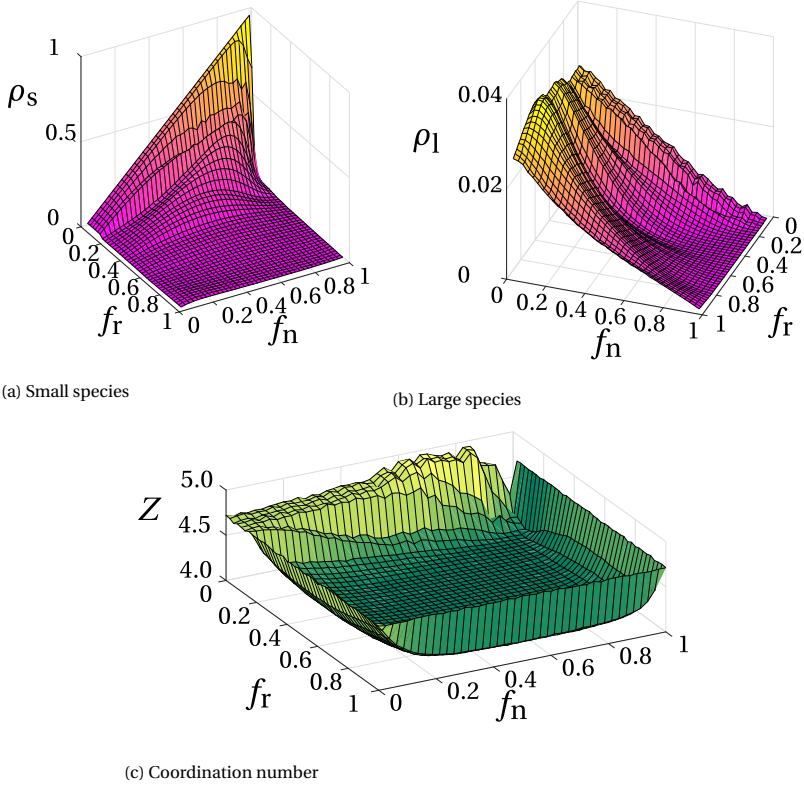
(a) Small species

(b) Large species

(c) Coordination number

Figure 4.4: (a) and (b) Fraction of small (ρ_s) and large (ρ_l) rattlers. Monodisperse edges are cut away; note the different orientation of (b). (c) Mean coordination Z.

When f_r is small nearly all small particles are rattlers, and the load-bearing network is monodisperse. A defect-free triangular lattice of large particles can only form when the lattice is commensurate with the simulation box; incommensurate boxes generate defects, evident as fine structure in ϕ_c along the f_n-direction (see fig. 4.3a).

Two minima.– The commonly chosen mixture of $f_r = 1.4$ and $f_n = 0.5$ (marked **a** in fig. 4.3b) sits in the larger of two 'basins' in the ϕ_c surface. Close to point **a** we find the mixture with the lowest ϕ_c, around $f_r = 0.8$, $f_n = 0.5$, labeled **e** in fig. 4.3b. There is a second basin with its own local minimum around $f_r = 0.4$, $f_n = 0.2$, marked **b** in fig. 4.3b. To our knowledge this second minimum has not previously been observed in 2D packings. In 3D thermal systems there seem to be no minima inside the domain [100, 105]. In the following Section we present several measures indicating that packings in both basins have low structural order. One consequence is that these states are indeed appropriate for studies of jamming.

Rattlers and coordination number.– So far we have taken f_n to be the fraction of small particles. While this is the relevant quantity when preparing packings experimentally, it is not for understanding the underlying load-bearing network. We have re-calculated the

ϕ_c surface using a corrected f_n – denoted f'_n – which is the number fraction of only the non-rattler particles (figs. 4.4a,4.4b). Using f'_n, the points **a** - **e** shift to the points labeled **a′** - **e′** (**f** and **f′** are the same, as it is monodisperse). The only significant shift is from **d** to **d′**, which sits in the region $f_r < f_r^*$ where rattlers are most prevalent.

The mean coordination number Z is a geometric measure with important consequences for mechanical response [2]. Counting arguments dating to Maxwell predict the isostatic value $Z_{iso} = 4$ in a disordered jammed disk mixture. Fig. 4.4c depicts Z averaged over the jammed states of our ensemble. Away from the monodisperse edges, there is a flat region in the Z surface with a height $Z \approx 4.1$, consistent with Maxwell. The difference from 4 is because our ensemble has a spread in the distance to jamming of individual packings. In the region $f_r < f_r^*$ and for lower f_n the Z surface is at the same height as the monodisperse edge, as all small particles are rattlers. Going to higher f_n we start seeing the effects of small particles jamming in the voids of the large particle crystal.

4.3. LOCAL ORDER

Order in a packing can be characterized by many different order parameters [96]. In monodisperse packings we find large patches with triangular lattice structure, while in the basins relatively few triangles are present (*cf.* figs. 4.1f and 4.1a). To characterize this local order, we count the number of triangles formed by three particles in contact normalized by the number of non-rattler particles in the packing. Figure 4.5a shows this measure for all mixtures. Observe that indeed the peak and ridge have a high count of triangles and are therefore relatively ordered. The basins, including the commonly used point $f_r = 1.4$ and $f_n = 0.5$, indeed have a low count of triangles, indicating lower structural order.

Surprisingly, we find the fewest triangles per particle near the local minimum **b** rather than the global minimum **e**, where ϕ_c is lower. Point **b** seems to be optimal for frustrating the triangular crystalline structure of the large particles – which, recall, is the reason point **a** is commonly selected. Therefore point **b** could be an interesting alternative to the widely studied point **a**. Packings at **b** differ from those at **a**/**e** in that the small species particles are smaller and there are fewer of them.

Even when triangles are present, they can form a disordered tiling. Such disorder is introduced when many triangles are formed by particles of both species. In these packings four different shapes and sizes of triangles make up a large part of the contact network, resulting in highly disordered structures. Figure 4.5d shows the number of 'mixed' triangles in which both species participate, again normalized with the number of non-rattlers. There is a curve of maximal mixed triangles that passes through the global minimum of ϕ_c. This suggests there is a qualitative difference in the disorder near the two minima.

One way to rationalize the curve of maximal mixed triangles is inspired by the intuitive idea that it is most likely to find a particle of the other species as a neighbor when the volume occupied by the species is roughly equal. The ratio between the volumes can be written as $V_a/V_b = f_r^2 f_n/(1 - f_n)$. For any such ratio we find curves of the form seen in fig. 4.3b; the dot-dashed curve, in particular, indicates mixtures for which the ratio is unity. This curve closely follows the ridge in the number of mixed triangles. We further note that the curves of constant volume ratio converge around the peak. Plotting ϕ_c along
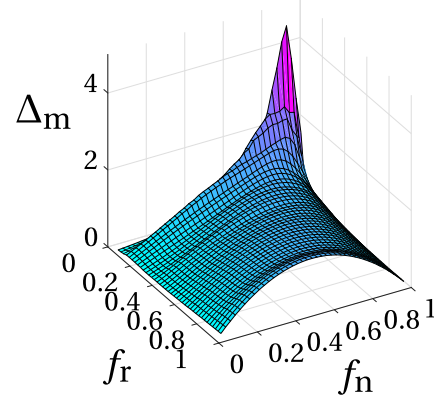
4
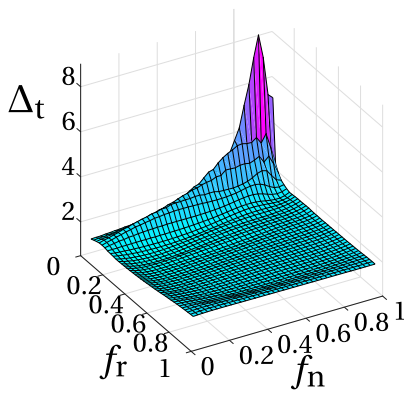
(a) Total count
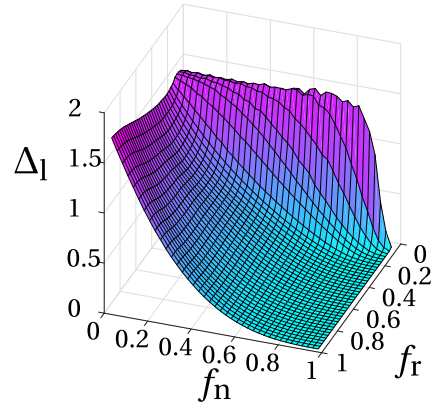
(b) Large species
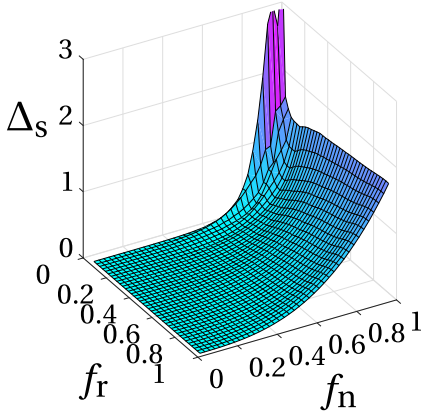
(c) Small species

(d) Mixed species

Figure 4.5: The number of triangles per non-rattler particle, one measure of crystallinity. Note that the monodisperse edge is cut away and the orientation of (b) is different.
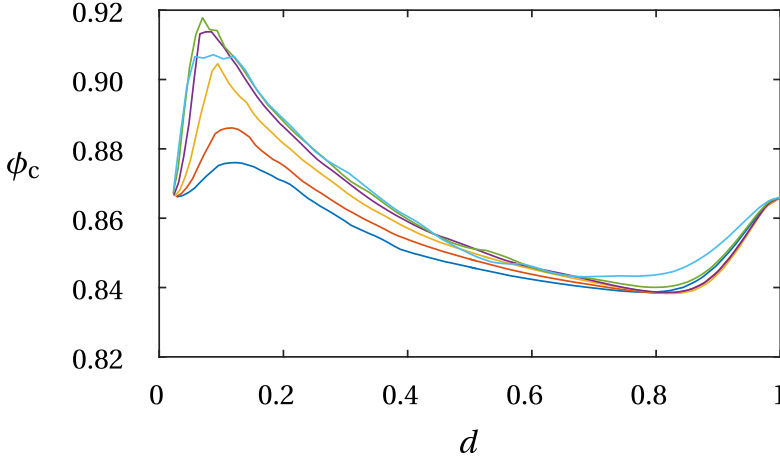
Figure 4.6: ϕ_c plotted along curves of constant volume ratio (dashed lines in fig. 4.3b). d is the relative distance along the curves.

the curves produces similar profiles with the peak and minimum in roughly the same location, see fig. 4.6.

4.4. STIFFNESS

States below the jamming transition are not rigid and cannot bear load, hence their stiffness or bulk modulus K is zero. However, when the jamming transition is approached from above K tends to a positive value [1]. Here we present K for all bidisperse mixtures, computed by applying a small volumetric strain to an ensemble of initially jammed packings and minimizing the energy. From the change in pressure p we determine the modulus as $K = (1/\phi)(dp/d\phi)$. As in experiments, a small number of contact changes can occur during the compression step, but numerical tests indicate that the ensemble-averaged modulus is unaffected [22, 87].

We plot the bulk modulus surface in fig. 4.7. Packings on the monodisperse edge have the same stiffness, as expected. States in the interior where $f_r > f_r^*$ show little difference from the monodisperse mixture. However there is a sharp increase in K in the region where small particles fit inside voids of triangles of touching large particles. The stiffest packings occur for low f_r and high f_n.

At the monodisperse limit there is a sharp increase in the stiffness. To determine if the increase is discontinuous, we take smaller steps towards this limit in a cross section with fixed $f_r = 0.6$. While true discontinuities can only be found in the large system size limit, we find that the increase in K becomes sharper with increasing N (see fig. 4.8). This indeed suggests there is a discontinuity in the bulk modulus K at the edge, while the critical packing fraction ϕ_c goes to the monodisperse limit continuously.

We caution that one must be careful when comparing the moduli and stresses of systems with different bidisperse mixtures, as varying f_r and f_n has two distinct effects.
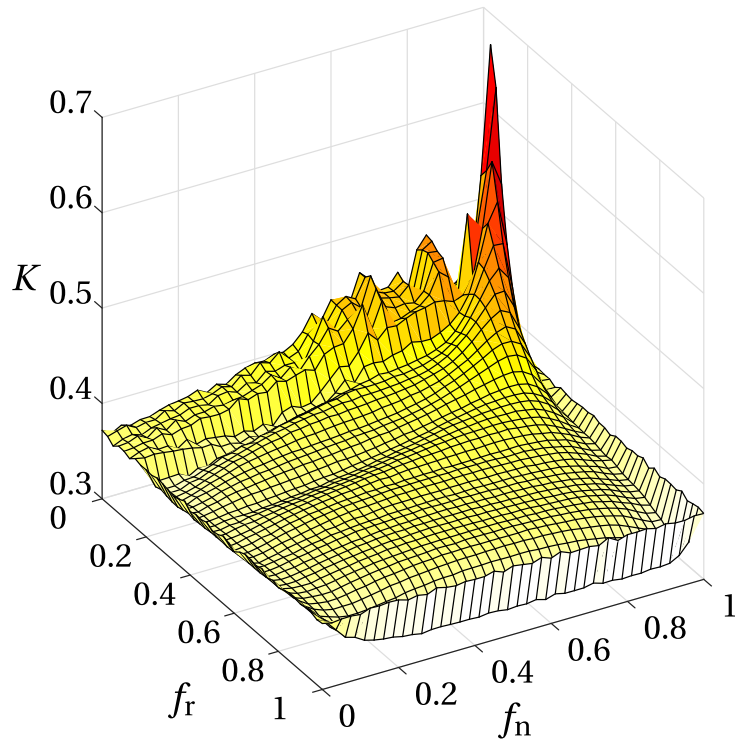
Figure 4.7: Bulk modulus for all size ratios f_r and number ratios f_n.
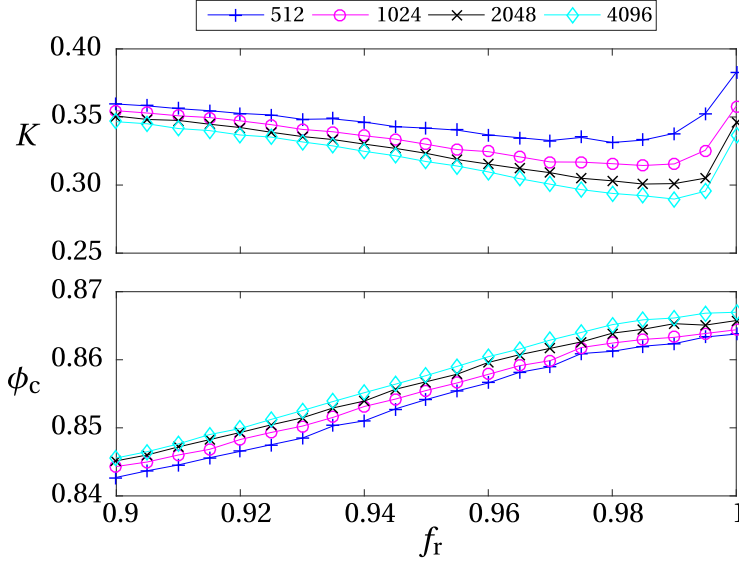
Figure 4.8: A cross section of the critical packing fraction ϕ_c and the bulk modulus B near the monodisperse edge. This cross section is for a fixed value of $f_n = 0.5$.

The first, which we probe in fig. 4.7, is the collective effect of structural differences in the contact network due to changes in the mixture composition and particle size ratio. The second effect is due to the fact that stress carries units of energy per unit volume, and is therefore sensitive both to an overall rescaling of the particle sizes, and to differences in box volume for different (f_r, f_n) at fixed N. The second effect can be quite large, as there is a factor 40 difference in the volume of a packing in the peak and one in the opposite corner of the ϕ_c landscape.

The natural units of stress are given by k_{eff}/R^{D-2}, where R is the typical particle size and the effective spring constant $k_{\mathrm{eff}} = f/\delta$ is determined by the ratio of the typical force f on a contact and the typical dimensionful overlap δ between particles. For disks interacting via the potential in eq. 4.1 the effective spring constant is simply k and the quantity R^{D-2} is simply unity, and hence the natural units of stress are constant. However for other values of the spatial dimension D, and/or other forms of the pair potential, the quantity k_{eff}/R^{D-2} will generally be sensitive to changes in R and/or the box volume. This is the case, *e.g.* , for the widely-used potential [1, 2, 77, 86, 88, 97]

$$U_{ij} = \frac{\epsilon}{2}\left(1 - \frac{r_{ij}}{R_i + R_j}\right)^2, \tag{4.2}$$

where ϵ is a constant with units of energy and the quantity in parentheses is the dimensionless overlap.
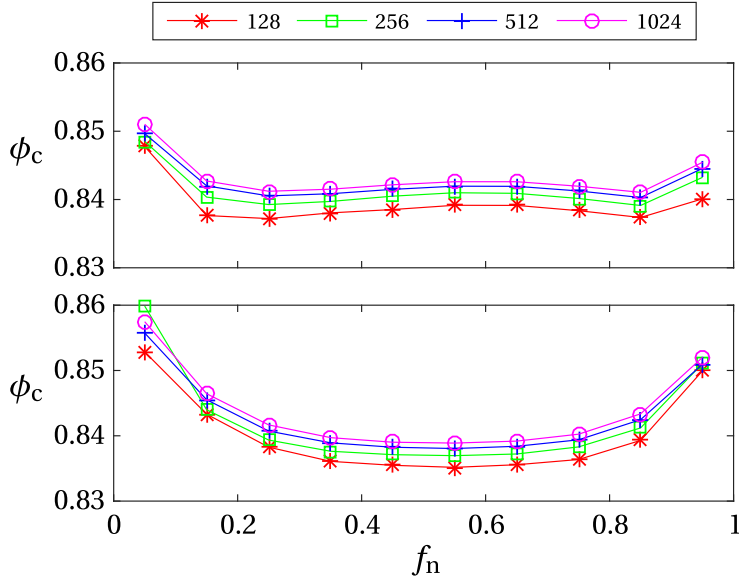
Figure 4.9: Finite size effects for two cross sections with fixed f_r at 0.45 and 0.65.

4.5. FINITE SIZE EFFECTS

The structure in ϕ_c remains the same in the infinite system limit. Figure 4.9 shows ϕ_c for two cross sections in the parameter space. We see that the cross sections uniformly increase in ϕ_c with increasing N. This shift converges with N, as apparent for the selected points from fig. 4.3b plotted in fig. 4.10. This means that the surface shifts upwards slightly, while retaining the features, *i.e.* the peak, two minima, the ridge and the monodisperse edges. For an extensive study of these finite-size effects for a certain mixture see *e.g.* [83].

We furthermore see that the fraction f_j of jammed packings has a sigmoidal shape (see fig. 4.2) that tends to a step function with increasing N [1, 88]. Since the surface only shifts we find that the sigmoidal shape of f_j goes to a step function with increasing N in the same way for all (f_r, f_n).

4.6. DISCUSSION

We have mapped out the critical packing fraction of all mixtures of bidisperse packings. We find that there is large region in the (f_r, f_n) parameter space that avoids structural order, and is therefore suitable for studies of jamming. In this sense the classic mixture of $f_r = 1.4 (\equiv 0.71)$ and $f_n = 0.5$ is not special, which is a fortunate finding given that most numerical studies address just this one point in state space. Intriguingly, we find not one but two local minima in the ϕ_c surface. While the global minimum is close to the classic mixture, the other minimum is at lower f_r and f_n ($f_r = 0.4$ and $f_n = 0.2$); we suggest that it might provide a useful alternate to the classic mixture for future numerical studies.

The region at low f_r is distinguished by a high rattler fraction, increased structural
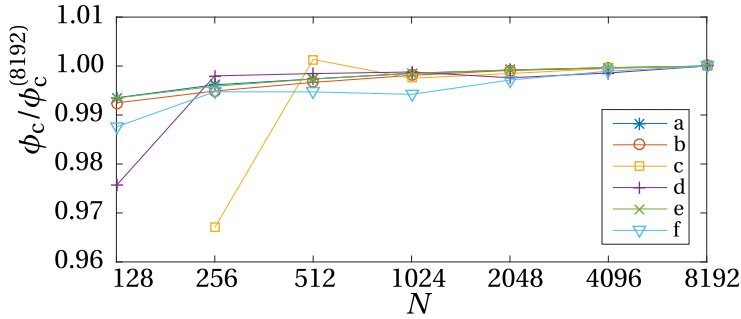
Figure 4.10: Finite size effects for the selected points in fig. 4.3b.

order, and enhanced stiffness. Mixtures from this region should not be selected as 'typical' disordered states. However, it may be possible to tune the packing stiffness by varying f_n in this region.

There is a number of ways to extend our results. 3D sphere packings are an obvious, albeit computationally expensive, direction; others include friction, particle shape, and other forms of polydispersity [106]. Alternative packing preparation protocols incorporating, e.g., thermal fluctuations, shear, or slow cooling, may cause the system to explore different energy minima than the infinitely fast quench employed here, thereby altering the ϕ_c landscape [1, 77, 100, 105]. It would also be worthwhile to verify the existence of the second minimum in ϕ_c experimentally (see also [104]). Systems that are close to our model include a monolayer of foam and trapped emulsions [107, 108].

CONCLUSIONS

A minimal model should be simple enough, but not too simple. For over a decade, researchers have painstakingly unraveled the physics of the soft sphere model in the vicinity of the jamming transition. We have thoroughly tested the minimal ingredients of the canonical model for jamming in two ways. The first is the use of a particular size distribution, and the second is the absence of attractive interactions.

The canonical soft sphere model uses 50:50 mixtures of purely repulsive bidisperse disks with 1.4:1 size ratio. We have systematically and simultaneously varied the size and number ratios in bidisperse packings. Our most important conclusion is that, within this parameter space, there exists a broad range of states that jam at similar packing fractions with similar mechanical and structural properties. Happily, the canonical number and size ratios sit squarely within this parameter regime. There is therefore good reason to expect that simulations using the canonical system are representative of the properties of other systems as well.

In addition, we have probed the role of attraction in jammed systems. We find that attraction has a strong influence on the jamming transition. Our most important conclusions are the following:

- *Attraction shifts the location of the transition.* Because particles can stick together, the system is capable of forming more tenuous, gel-like states that nevertheless support shear stress. Therefore the critical packing fraction is shifted downwards with respect to the purely repulsive jamming point. The stronger the attraction between particles, the greater the downward shift.

- *Attraction alters the order of the transition.* In repulsive jamming, a system-spanning rigid cluster emerges suddenly at the jamming point, while just below the transition the largest rigid cluster typically contains just a few particles. This is reminiscent of a first order equilibrium phase transition. In sharp contrast, in attractive systems rigid clusters grow continuously in size as the packing fraction is increased. There is no sharp jump in the size of the largest cluster when it spans the system. This is characteristic of a second order phase transition.

- *Sticky jammed solids have new elastic properties.* While the elasticity of repulsive jammed states has been exhaustively researched in computer models, the behavior of sticky systems near jamming remained almost entirely unexplored. We showed that the elastic moduli and coordination of sticky jammed solids display power law scaling with the distance to the jamming point, with critical exponents that differ significantly from their repulsive counterparts.

Sticky jamming is therefore *qualitatively different* from repulsive jamming. Importantly, attraction is also generic to most physical systems. Therefore, our work suggests that it should be incorporated as an essential element of the minimal model for jamming.

There are a number of likely future directions in which to continue this line of research. Examples include:

- Investigating the vibrational properties of states near an attractive jamming point. The vibrational density of states is intimately related to a number of mechanical and transport properties necessary to model processes. These include elastic moduli, sound speeds, and heat transfer coefficients.

- Characterizing viscoelastic properties. When systems are deformed at finite rate they dissipate energy. The balance between elastic "storage" and viscous "loss" is responsible for a number of material properties, including, e.g., our perception of "mouth feel" in food products. We expect that viscous loss also shows a critical dependence on proximity to jamming.

- Determining the effect of large deformations. This thesis has focused on small deformations where the stress remains proportional to the imposed strain. When systems are deformed further, the stress-strain relation becomes nonlinear. In soft solids, the amount of deformation needed to induce nonlinearity is often quite small. It is therefore important to determine how and when this occurs to model industrial processes.

- Exploring the role of protocol dependence and hysteresis. Once attractive particles form bonds, whether during preparation or subsequent deformation, they tend to remain bonded. This can promote strong hysteresis and/or protocol dependence. We have focused on one particular protocol and linear response, in which hysteresis does not occur. However, it is important to determine how other protocols influence computed material properties. As an example, many systems are prepared by subjecting them to a large pre-shear, which may alter the shear modulus.

REFERENCES

[1] C. S. O'Hern, L. E. Silbert, A. J. Liu, and S. R. Nagel, *Jamming at zero temperature and zero applied stress: The epitome of disorder,* Phys. Rev. E **68**, 011306 (2003).

[2] M. van Hecke, *Jamming of soft particles: Geometry, mechanics, scaling and isostaticity,* J. Phys. Cond. Matt. **22**, 033101 (2010).

[3] D. J. Jacobs and M. F. Thorpe, *Generic rigidity percolation: the pebble game,* Phys. Rev. Lett. **75**, 4051 (1995).

[4] A. V. Tkachenko and T. A. Witten, *Stress propagation through frictionless granular material,* Phys. Rev. E **60**, 687 (1999).

[5] J.-N. Roux, *Geometric origin of mechanical properties of granular materials,* Phys. Rev. E **61**, 6802 (2000).

[6] B. P. Tighe, *Relaxations and rheology near jamming,* Phys. Rev. Lett. **107**, 158303 (2011).

[7] C. H. Liu, S. R. Nagel, D. A. Schecter, S. N. Coppersmith, S. Majumdar, O. Narayan, and T. A. Witten, *Force fluctuations in bead packs,* Science **269**, 513 (1995).

[8] J. Maxwell, *On the calculation of the equilibrium and stiffness of frames,* Philosoph. Mag. **27**, 294 (1864).

[9] S. Pellegrino and C. R. Calladine, *Matrix analysis of statically and kinematically indeterminate frameworks,* Int. J. Solids Structures **22**, 409 (1986).

[10] T. G. Roberts, S. J. Cox, A. L. Lewis, and S. A. Jones, *Characterisation and optimisation of foams for varicose vein sclerotherapy,* Biorheology **57**, 77 (2021).

[11] A. Deblais, E. d. Hollander, C. Boucon, A. E. Blok, B. Veltkamp, P. Voudouris, P. Versluis, H.-J. Kim, M. Mellema, M. Stieger, *et al.*, *Predicting thickness perception of liquid food products from their non-newtonian rheology,* Nature communications **12**, 1 (2021).

[12] A. Hemmerle, M. Schröter, and L. Goehring, *A cohesive granular material with tunable elasticity,* Scientific Reports **6**, 35650 (2016).

[13] S. V. Franklin and M. D. Schattuck, eds., *Handbook of Granular Materials* (CRC Press, 2015).

[14] D. J. Durian, *Foam mechanics at the bubble scale,* Phys. Rev. Lett. **75**, 4780 (1995).

[15] A. J. Liu and S. R. Nagel, *The jamming transition and the marginally jammed solid,* Ann. Rev. Cond. Matt. Phys. **1**, 347 (2010).

[16] M. Wyart, L. E. Silbert, S. R. Nagel, and T. A. Witten, *Effects of compression on the vibrational modes of marginally jammed solids,* Phys. Rev. E **72**, 051306 (2005).

[17] M. Wyart, *On the rigidity of amorphous solids,* Annales de Physique **30**, 1 (2005).

[18] W. G. Ellenbroek, M. van Hecke, and W. van Saarloos, *Jammed frictionless disks: Connecting local and global response,* Phys. Rev. E **80**, 061307 (2009).

[19] P. Olsson and S. Teitel, *Critical scaling of shear viscosity at the jamming transition,* Phys. Rev. Lett. **99**, 178001 (2007).

[20] A. Ikeda, L. Berthier, and P. Sollich, *Unified study of glass and jamming rheology in soft particle systems,* Phys. Rev. Lett. **109**, 018301 (2012).

[21] H. Mizuno, K. Saitoh, and L. E. Silbert, *Elastic moduli and vibrational modes in jammed particulate packings,* Physical Review E **93**, 062905 (2016).

[22] J. Boschan, D. Vågberg, E. Somfai, and B. P. Tighe, *Beyond linear elasticity: Jammed solids at finite shear strain and rate,* Soft Matter **12**, 5450 (2016).

[23] K. Baumgarten and B. P. Tighe, *Viscous forces and bulk viscoelasticity near jamming,* Soft Matter **13**, 8368 (2017).

[24] D. L. Weaire and S. Hutzler, *The Physics of Foams* (Oxford University Press, Oxford, 2001).

[25] L. Bécu, S. Manneville, and A. Colin, *Yielding and flow in adhesive and nonadhesive concentrated emulsions,* Phys. Rev. Lett. **96**, 138302 (2006).

[26] I. Jorjadze, L.-L. Pontani, K. A. Newhall, and J. Brujić, *Attractive emulsion droplets probe the phase diagram of jammed granular matter,* Proc. Nat. Acad. Sci. (USA) **108**, 4286 (2011).

[27] S. Herminghaus, *Dynamics of wet granular matter,* Advances in Physics **54**, 221 (2005).

[28] P. C. Møller and D. Bonn, *The shear modulus of wet granular matter,* Europhys. Lett. **80**, 38002 (2007).

[29] P. J. Yunker, K. Chen, Z. Zhang, and A. G. Yodh, *Phonon spectra, nearest neighbors, and mechanical stability of disordered colloidal clusters with attractive interactions,* Phys. Rev. Lett. **106**, 225503 (2011).

[30] D. Vella and L. Mahadevan, *The "cheerios effect",* Am. J. Phys. **73**, 817 (2005).

[31] S. Karpitschka, A. Pandey, L. A. Lubbers, J. H. Weijs, L. Botto, S. Das, B. Andreotti, and J. H. Snoeijer, *Liquid drops attract or repel by the inverted cheerios effect,* Proc. Nat. Acad. Sci. (USA) **113**, 7403 (2016).

[32] D. Bonn, J. Otwinowski, S. Sacanna, H. Guo, G. Wegdam, and P. Schall, *Direct observation of colloidal aggregation by critical casimir forces,* Phys. Rev. Lett. **103**, 156101 (2009).

[33] D. Head, *Well defined transition to gel–like aggregates of attractive athermal particles,* Eur. Phys. J. E **22**, 151 (2007).

[34] W. Zheng, H. Liu, and N. Xu, *Shear-induced solidification of athermal systems with weak attraction,* Phys. Rev. E **94**, 062608 (2016).

[35] P. Chaudhuri, L. Berthier, and L. Bocquet, *Inhomogeneous shear flows in soft jammed materials with tunable attractive forces,* Phys. Rev. E **85**, 021503 (2012).

[36] E. Irani, P. Chaudhuri, and C. Heussinger, *Impact of attractive interactions on the rheology of dense athermal particles,* Phys. Rev. Lett. **112**, 188303 (2014).

[37] E. Irani, P. Chaudhuri, and C. Heussinger, *Athermal rheology of weakly attractive soft particles,* Phys. Rev. E **94**, 052608 (2016).

[38] T. Yamaguchi and A. Faraone, *Analysis of shear viscosity and viscoelastic relaxation of liquid methanol based on molecular dynamics simulation and mode-coupling theory,* J. Chem. Phys. **146**, 244506 (2017).

[39] G. Lois, J. Blawzdziewicz, and C. S. O'Hern, *Jamming transition and new percolation universality classes in particulate systems with attraction,* Phys. Rev. Lett. **100**, 028001 (2008).

[40] W. G. Ellenbroek, V. F. Hagh, A. Kumar, M. Thorpe, and M. Van Hecke, *Rigidity loss in disordered systems: Three scenarios,* Phys. Rev. Lett. **114**, 135501 (2015).

[41] S. Henkes, D. A. Quint, Y. Fily, and J. M. Schwarz, *Rigid cluster decomposition reveals criticality in frictional jamming,* Phys. Rev. Lett. **116**, 028301 (2016).

[42] D. J. Koeze, D. Vågberg, B. B. Tjoa, and B. P. Tighe, *Mapping the jamming transition of bidisperse mixtures,* Europhys. Lett. **113**, 54001 (2016).

[43] A. A. Saberi, *Recent advances in percolation theory and its applications,* Physics Reports **578**, 1 (2015).

[44] S. E. Rahbari, J. Vollmer, S. Herminghaus, and M. Brinkmann, *Fluidization of wet granulates under shear,* Phys. Rev. E **82**, 061305 (2010).

[45] J. Gu, M. Song, S. Ni, X. Liao, and S. Guo, *Improving the plasticity of bulk metallic glasses via pre-compression below the yield stress,* Mat. Sci. and Eng.: A **602**, 68 (2014).

[46] B. P. Tighe, E. Woldhuis, J. J. C. Remmers, W. van Saarloos, and M. van Hecke, *Model for the scaling of stresses and fluctuations in flows near jamming,* Phys. Rev. Lett. **105**, 088303 (2010).

[47] S. Dagois-Bohy, E. Somfai, B. Tighe, and M. van Hecke, *Softening and yielding of soft glassy materials,* Soft Matter **13**, 9036 (2017).

[48] L. Bocquet, A. Colin, and A. Ajdari, *Kinetic theory of plastic flow in soft glassy materials,* Phys. Rev. Lett. **103**, 036001 (2009).

[49] K. Baumgarten, D. Vågberg, and B. P. Tighe, *Nonlocal elasticity near jamming in frictionless soft spheres,* Phys. Rev. Lett. **118**, 098001 (2017).

[50] Z. Tang, T. A. Brzinski, M. Shearer, and K. E. Daniels, *Nonlocal rheology of dense granular flow in annular shear experiments,* Soft Matter **14**, 3040 (2018).

[51] A. Singh, V. Magnanimo, K. Saitoh, and S. Luding, *Effect of cohesion on shear banding in quasistatic granular materials,* Phys. Rev. E **90**, 022202 (2014).

[52] V. Trappe, V. Prasad, L. Cipelletti, P. Segre, and D. A. Weitz, *Jamming phase diagram for attractive particles,* Nature **411**, 772 (2001).

[53] V. Trappe and P. Sandkühler, *Colloidal gels—low-density disordered solid-like states,* Current Opinion in Colloid & Interface Science **8**, 494 (2004).

[54] H. Tanaka, J. Meunier, and D. Bonn, *Nonergodic states of charged colloidal suspensions: repulsive and attractive glasses and gels,* Phys. Rev. E **69**, 031404 (2004).

[55] L. Berthier and T. A. Witten, *Glass transition of dense fluids of hard and compressible spheres,* Phys. Rev. E **80**, 021502 (2009).

[56] M. R. Hestenes and E. Stiefel, *Methods of conjugate gradients for solving linear systems*, Vol. 49 (NBS, Washington, DC, 1952).

[57] R. Fletcher and C. M. Reeves, *Function minimization by conjugate gradients,* The Computer Journal **7**, 149 (1964).

[58] M. J. D. Powell, *Restart procedures for the conjugate gradient method,* Mathematical Programming **12**, 241 (1977).

[59] N. J. Higham, *Accuracy and stability of numerical algorithms*, Vol. 80 (Siam, 2002).

[60] B. Serpette, J. Vuillemin, and J.-C. Hervé, *BigNum: a portable and efficient package for arbitrary-precision arithmetic* (Digital. Paris Research Laboratory, 1989).

[61] J. R. Shewchuk, *Adaptive precision floating-point arithmetic and fast robust geometric predicates,* Discrete & Computational Geometry **18**, 305 (1997).

[62] *GNU Multiple Precision Arithmetic Library,* Gmplib.org.

[63] D. M. Priest, *Algorithms for arbitrary precision floating point arithmetic,* in *Computer Arithmetic, 1991. Proceedings., 10th IEEE Symposium on* (IEEE, 1991) pp. 132–143.

[64] Y. Hida, X. S. Li, and D. H. Bailey, *Quad-double arithmetic: Algorithms, implementation, and application,* in *15th IEEE Symposium on Computer Arithmetic* (Citeseer, 2000) pp. 155–162.

[65] *GCC Quadmath Library,* Gcc.gnu.org/onlinedocs/libquadmath.

[66] A. J. Liu and S. R. Nagel, *Nonlinear dynamics: Jamming is not just cool any more,* Nature **396**, 21 (1998).

[67] I. Golovkova, L. Montel, E. Wandersman, T. Bertrand, A. M. Prevost, and L.-L. Pontani, *Depletion attraction impairs the plasticity of emulsions flowing in a constriction,* Soft Matter **16**, 3294 (2020).

[68] S. Cox, A. Kraynik, D. Weaire, and S. Hutzler, *Ideal wet two-dimensional foams and emulsions with finite contact angle,* Soft Matter **14**, 5922 (2018).

[69] E. Koos and N. Willenbacher, *Capillary forces in suspension rheology,* Science **331**, 897 (2011).

[70] G. Katgert, B. P. Tighe, and M. van Hecke, *The jamming perspective on wet foams,* Soft Matter **9**, 9739 (2013).

[71] D. J. Koeze and B. P. Tighe, *Sticky matters: Jamming and rigid cluster statistics with attractive particle interactions,* Phys. Rev. Lett. **121**, 188002 (2018).

[72] S. Alexander, *Amorphous solids: their structure, lattice dynamics and elasticity,* Phys. Rep **296**, 65 (1998).

[73] B. P. Tighe and T. J. H. Vlugt, *Stress fluctuations in granular force networks,* J. Stat. Mech.: Theory and Experiment **2011**, P04002 (2011).

[74] E. Lerner, G. Düring, and M. Wyart, *A unified framework for non-brownian suspension flows and soft amorphous solids,* Proc. Nat. Acad. Sci. (USA) **109**, 4798 (2012).

[75] J. Paulose, A. S. Meeussen, and V. Vitelli, *Selective buckling via states of self-stress in topological metamaterials,* Proc. Nat. Acad. Sci. (USA) **112**, 7639 (2015).

[76] C. E. Maloney and A. Lemaître, *Amorphous systems in athermal, quasistatic shear,* Phys. Rev. E **74**, 016118 (2006).

[77] D. Vågberg, P. Olsson, and S. Teitel, *Glassiness, rigidity, and jamming of frictionless soft core disks,* Phys. Rev. E **83**, 031307 (2011).

[78] M. Merkel, K. Baumgarten, B. P. Tighe, and M. L. Manning, *A minimal-length approach unifies rigidity in underconstrained materials,* Proc. Nat. Acad. Sci. (USA) **116**, 6560 (2019).

[79] W. G. Ellenbroek, Z. Zeravcic, W. van Saarloos, and M. van Hecke, *Non-affine response: Jammed packings vs. spring networks,* Europhys. Lett. **87**, 34004 (2009).

[80] M. Schlegel, J. Brujic, E. Terentjev, and A. Zaccone, *Local structure controls the nonaffine shear and bulk moduli of disordered solids,* Scientific Reports **6**, 18724 (2016).

[81] C. P. Goodrich, A. J. Liu, and S. R. Nagel, *Finite-size scaling at the jamming transition,* Phys. Rev. Lett. **109**, 095704 (2012).

[82] S. Dagois-Bohy, B. P. Tighe, J. Simon, S. Henkes, and M. van Hecke, *Soft-sphere packings at finite pressure but unstable to shear,* Phys. Rev. Lett. **109**, 095703 (2012).

[83] C. P. Goodrich, S. Dagois-Bohy, B. P. Tighe, M. van Hecke, A. J. Liu, and S. R. Nagel, *Jamming in finite systems: Stability, anisotropy, fluctuations, and scaling,* Phys. Rev. E **90**, 022138 (2014).

[84] S. Feng, M. Thorpe, and E. Garboczi, *Effective-medium theory of percolation on central-force elastic networks,* Phys. Rev. B **31**, 276 (1985).

[85] K. Saitoh, T. Hatano, A. Ikeda, and B. P. Tighe, *Stress relaxation above and below the jamming transition,* Phys. Rev. Lett. **124**, 118001 (2020).

[86] D. Vågberg, Y. Wu, P. Olsson, and S. Teitel, *Pressure distribution and critical exponent in statically jammed and shear-driven frictionless disks,* Phys. Rev. E **89**, 022201 (2014).

[87] M. S. van Deen, J. Simon, Z. Zeravcic, S. Dagois-Bohy, B. P. Tighe, and M. van Hecke, *Contact changes near jamming,* Phys. Rev. E **90**, 020202 (2014).

[88] D. Vågberg, D. Valdez-Balderas, M. A. Moore, P. Olsson, and S. Teitel, *Finite-size scaling at the jamming transition: Corrections to scaling and the correlation-length critical exponent,* Phys. Rev. E **83**, 030303 (2011).

[89] S. Luding, *Liquid-solid transition in bidisperse granulates,* Advs. Complex Syst. **4**, 379 (2001).

[90] T. Ueda, T. Matsushima, and Y. Yamada, *Effect of particle size ratio and volume fraction on shear strength of binary granular mixture,* Gran. Matter. **13**, 731 (2011).

[91] J. D. Bernal, *A geometrical approach to the structure of liquids,* Nature **183**, 141 (1959).

[92] G. P. Bierwagen and T. E. Saunders, *Studies of the effects of particle size distribution on the packing efficiency of particles,* Powder Tech. **10**, 111 (1974).

[93] D. R. Nelson, M. Rubinstein, and F. Spaepen, *Order in two-dimensional binary random arrays,* Phil. Mag. A **46**, 105 (1982).

[94] D. R. Nelson, *Orientational ordering in 2- and 3-dimensional systems,* J. of Non-Cryst. Sol. **61 & 62**, 475 (1984).

[95] M. Rubinstein and D. R. Nelson, *Order and deterministic chaos in hard-disk arrays,* Phys. Rev. B **26**, 11 (1982).

[96] S. Torquato, T. M. Truskett, and P. G. Debenedetti, *Is random close packing of spheres well defined?* Phys. Rev. Lett. **84**, 2064 (2000).

[97] D. N. Perera and P. Harrowell, *Stability and structure of a supercooled liquid mixture in two dimensions,* Phys. Rev. E **59**, 5721 (1999).

[98] R. J. Speedy, *Glass transition in hard disc mixtures,* J. Chem. Phys. **110**, 9 (1999).

[99] A. Donev, I. Cisse, D. Sachs, E. A. Variano, F. H. Stillinger, R. Connelly, S. Torquato, and P. M. Chaikin, *Improving the density of jammed disordered packings using ellipsoids,* Science **303**, 990 (2004).

[100] N. Kumar, V. Magnanimo, M. Ramaioli, and S. Luding, *Tuning the bulk properties of bidisperse granular mixtures by small amount of fines,* Powder Technology **293**, 94 (2016).

[101] V. Ogarko and S. Luding, *Equation of state and jamming density for equivalent bi- and polydisperse, smooth, hard sphere systems,* J. Chem. Phys. **136**, 124508 (2012).

[102] S.-C. Zhao, S. Sidle, H. L. Swinney, and M. Schröter, *Correlation between Voronoi volumes in disc packings,* Europhys. Lett. **97**, 34004 (2012).

[103] S.-C. Zhao and M. Schröter, *Measuring the configurational temperature of a binary disc packing,* Soft Matter **10**, 4208 (2014).

[104] J. G. Puckett, F. Lechenault, and K. E. Daniels, *Local origins of volume fraction fluctuations in dense granular materials,* Phys. Rev. E **83**, 041301 (2011).

[105] I. Biazzo, F. Caltagirone, G. Parisi, and F. Zamponi, *Theory of amorphous packings of binary mixtures of hard spheres,* Phys. Rev. Lett. **102**, 195701 (2009).

[106] E. R. Chen, D. Klotsa, M. Engel, P. F. Damasceno, and S. C. Glotzer, *Complexity in surfaces of densest packings for families of polyhedra,* Phys. Rev. X **4**, 011024 (2014).

[107] G. Katgert and M. van Hecke, *Jamming and geometry of two-dimensional foams,* Europhys. Lett. **92**, 34002 (2010).

[108] K. W. Desmond, P. J. Young, D. Chen, and E. R. Weeks, *Experimental study of forces between quasi-two-dimensional emulsion droplets near jamming,* Soft Matter **9**, 3424 (2013).

CURRICULUM VITÆ

Dionysius Johannes KOEZE

20-07-1988   Born in Woerden, Netherlands.

EDUCATION

2000–2006	Grammar School	WolfertDalton, Rotterdam
2006–2009	Delft University of Technology	B.Sc. Applied Physics
2009–2012	Delft University of Technology	M.Sc. Applied Physics
2009–2012	Delft University of Technology	M.Sc. Applied Mathematics

LIST OF PUBLICATIONS

4. **D.J. Koeze, L. Hong, A. Kumar, and B.P. Tighe**, *Elasticity of jammed packings of sticky disks*, Physical Review Research **2**, 032047(R) (2020).

3. **D.J. Koeze and B.P. Tighe**, *Sticky Matter: Jamming and rigid cluster statistics with attractive particle interactions*, Physical Review Letters **121**, 188002 (2018).

2. [†]**R. Dekker, M. Dinkgreve, D.J Koeze, B.P. Tighe, H. de Cagny, and D. Bonn**, *Universal scaling of flow curves: comparison between experiments and simulations*, Journal of Non-Newtonian Fluid Mechanics **261**, 33-37 (2018).

1. **D.J. Koeze, D. Vågberg, B.B.T. Tjoa, and B.P. Tighe**, *Mapping the jamming transition of bidisperse mixtures*, Europhysics Letters **113**, 54001 (2016).

[†] Does not appear in this thesis.

ACKNOWLEDGEMENTS

This work has come together with the direct and indirect help of many people, whom I would like to thank here.

First of all I would like to deeply thank my promotores Brian and Thijs. I enjoyed working with you and have learned a great deal from you. It was very valuable to me to have the autonomy and freedom to pursue the topics of my interest.

Brian, I want to emphasize my gratitude for our day-to-day work. Besides your helpful insights and expansive knowledge of the literature, I enjoyed getting distracted (perhaps a bit too much) by our conversations on the daily observations of cultural and linguistic differences that go unnoticed to most.

There was some serious motivational effort required on my part to finalize this work. Thank you, Thijs, for giving me the final push, without this it might not have happened.

I would like to sincerely thank all co-authors, Abhishek, Boy, Daniel, Daniel, Henri, Ling, Maureen, and Riande, for our fruitful and pleasant co-operation.

Working with the 'jamming group', Daniel, Julia, Karsten has been a pleasure. Daniel, I loved our train trips and hikes all over The Netherlands. Julia, there surely is no topic in politics we have not fervently discussed. Karsten, we've had an awesome time in Boulder.

Working with everyone in, around and beyond the Engineering Thermodynamics group was a pleasure. I still remember the magical *schoolreisjes* to the Efteling. I would like to especially thank Ahmadreza, Ali, Burak, Carlos, Christos, Hirad, Hongxia, Jurriaan, Mahinder, Mariette, Marloes, Mate, Meng, Noura, Othon, Remco, Remco, Sebastian, Seyed, Tim, Vilborg, and Weiwei.

Perhaps without their knowledge, I feel greatly indebted to my paranimphs. There have been many occasions where I have thought back with a smile on my face how we, Ronald and I, have kept ourselves motivated during tedious physics experiments. Emile, we can go to extreme lengths to disprove each other in the most varied discussions, but I feel we do it with love.

Finally I would like to express my heartfelt gratitude towards Krispijn, my parents and Yoena and Joren for unconditionally supporting me and enabling me to follow my own way in pursuing this PhD and in life in general.